



PAPER

Ab initio electronic structure and prospects for the formation of ultracold calcium–alkali-metal-atom molecular ions

OPEN ACCESS

RECEIVED

20 February 2020

REVISED

6 May 2020

ACCEPTED FOR PUBLICATION

18 May 2020

PUBLISHED

15 July 2020

Original content from this work may be used under the terms of the [Creative Commons Attribution 4.0 licence](#).

Any further distribution of this work must maintain attribution to the author(s) and the title of the work, journal citation and DOI.

Wissem Zrafi¹, Hela Ladjimi¹, Halima Said¹, Hamid Berriche^{1,2}  and Michał Tomza³ ¹ Laboratory of Interfaces and Advanced Materials, Physics Department, Faculty of Science, University of Monastir, Avenue de l'Environnement, 5019 Monastir, Tunisia² Department of Mathematics and Natural Sciences, School of Arts and Sciences, American University of Ras Al Khaimah, Ras Al Khaimah, United Arab Emirates³ Faculty of Physics, University of Warsaw, Pasteura 5, 02-093 Warsaw, PolandE-mail: hamidberriche@yahoo.fr and michal.tomza@fuw.edu.pl**Keywords:** cold ion–atom mixtures, molecular ions, charge transfer, radiative association, electronic structure, ultracold collisions Supplementary material for this article is available [online](#)

Abstract

Experiments with cold ion–atom mixtures have recently opened the way for the production and application of ultracold molecular ions. Here, in a comparative study, we theoretically investigate ground and several excited electronic states and prospects for the formation of molecular ions composed of a calcium ion and an alkali-metal atom: CaAlk^+ ($\text{Alk} = \text{Li}, \text{Na}, \text{K}, \text{Rb}, \text{Cs}$). We use a quantum chemistry approach based on non-empirical pseudopotentials, operatorial core-valence correlation, large Gaussian basis sets, and full configuration interaction method for valence electrons. Adiabatic potential energy curves, spectroscopic constants, and transition and permanent electric dipole moments are determined and analyzed for the ground and excited electronic states. We examine the prospects for ion-neutral reactive processes and the production of molecular ions via spontaneous radiative association and laser-induced photoassociation. After that, spontaneous and stimulated blackbody radiation transition rates are calculated and used to obtain radiative lifetimes of vibrational states of the ground and first-excited electronic states. The present results pave the way for the formation and spectroscopy of calcium–alkali-metal-atom molecular ions in modern experiments with cold ion–atom mixtures.

1. Introduction

Cold mixtures of alkaline-earth-metal ions and alkali-metal atoms have recently emerged as a new field of research at the crossroad of quantum physics and chemistry [1–3]. Hybrid systems of trapped ions and ultracold atoms combined in a single experimental setup have opened the way for exciting applications ranging from studying cold collisions [4–8] and controlled chemical reactions [9–15] to quantum simulation of solid-state physics [16–18] and quantum computation [19]. Most of the cold ion–atom experiments use alkaline-earth-metal ions and alkali-metal or alkaline-earth-metal atoms because of their electronic structure favorable for laser cooling. Several cold atomic ion–atom combinations have already been experimentally investigated, including Yb^+/Yb [20], Ca^+/Rb [21], Ba^+/Ca [22], Yb^+/Ca [23], Yb^+/Rb [5], Ca^+/Li [24], Ca^+/Rb [25], Ca^+/Na [26], Sr^+/Rb [27], Yb^+/Li [12], Ca^+/K [28], Ba^+/Rb [29], and Rb^+/Rb [6, 30]. Ca^+ ions are the most common choice because advanced methods of their manipulation and detection have been developed for quantum simulation and computation applications [31, 32].

In cold ion–atom mixtures, diatomic molecular ions can be produced via collision-induced charge-transfer radiative association or light-induced photoassociation [10, 33–37]. The radiative association is predicted to dominate charge-transfer processes in most of the mixtures of alkaline-earth-metal ions and alkali-metal atoms. Until now, CaRb^+ [21, 25], BaRb^+ [38], CaYb^+ [23],

CaBa⁺ [22] molecular ions were observed as products of cold collisions between respective atomic ions and atoms. On the other hand, Rb₂⁺ [39] and Ca₂⁺ [40] molecular ions were formed by the photoionization of ultracold molecules. Molecular ions, which possess a ro-vibrational structure, can likewise be employed to realize cold, controlled ion–atom chemistry [41–45] and precision measurements [46, 47].

A mixture of Ca⁺ ions and Na atoms was considered in the pioneering proposal, which suggested combining ions trapped in a Paul trap with ultracold atoms [10]. Such mixture was later experimentally realized [26]. Coulomb crystals of Ca⁺ ions were immersed into ultracold Rb atoms to study radiative charge exchange and molecular ions formation [21, 25, 48]. Ca⁺ ions were also experimentally studied in mixtures with ultracold Li atoms [15, 24, 49, 50]. In fact, Ca⁺/Li ion–atom combination is one of the most promising systems for reaching the quantum regime of ion–atom collisions [8] due to the favorable mass ratio reducing the impact of micromotion-induced heating in hybrid traps [51]. Recently, a new apparatus with a mixture of laser-cooled Ca⁺ ions in a linear Paul trap overlapped with ultracold K atoms in a magneto-optical trap was presented [28, 52]. This setup incorporates a high-resolution time-of-flight mass spectrometer designed for radial extraction and detection of reaction products opening the way for detailed studies of the state-selected formation of CaK⁺ molecular ions. While, the electronic structure of the ground and excited electronic states was already studied for the CaLi⁺ [15, 53–58], CaNa⁺ [10, 53, 59, 60], and CaRb⁺ [35, 53, 61, 62] molecular ions and their neutral counterparts [63], to the best of our knowledge, the structure of excited electronic states of the CaK⁺ and CaCs⁺ molecular ions has not been presented, yet.

Here, to fill this gap, in a comparative study, we investigate the electronic structure of the group of five diatomic molecular ions composed of a Ca⁺ ion interacting with an alkali-metal atom: CaAlk⁺ (Alk = Li, Na, K, Rb, Cs). We calculate ground and several low-lying excited electronic states using a theoretical quantum chemistry approach based on non-empirical pseudopotentials, operatorial core-valence correlation, large Gaussian basis sets, and full configuration interaction method for valence electrons. Next, we employ electronic structure data to access prospects for field-free and light-assisted ion-neutral reactive processes and the formation of the considered molecular ions via spontaneous radiative association and laser-induced photoassociation. We discuss similarities and differences between considered systems. Finally, we calculate spontaneous and stimulated blackbody radiation transition rates together with radiative lifetimes of vibrational states of the ground and first excited electronic states.

This paper has the following structure. Section 2 describes the used computational methods. Section 3 presents and discusses obtained results, including electronic structure data and spontaneous charge transfer and radiative association rates. The radiative lifetimes of the ground and excited states are also presented there. The experimental implications of the presented calculations are analyzed in detail. To conclude, section 4 summarizes our work.

2. Computational details

In this work, we calculate non-relativistic potential energy curves within the Born–Oppenheimer approximation for the ground and excited electronic states of calcium–alkali-metal-atom molecular ions: CaAlk⁺ (Alk = Li, Na, K, Rb, Cs). To this end, we employ the *ab initio* approach, which was developed and presented previously in several works on alkali hydrides [64–67], alkali-metal dimers [68–71], alkaline-earth-metal hydrides [72–74], and alkali-metal–alkaline-earth-metal molecular ions [75, 76]. The investigated CaAlk⁺ molecular ions, thus, are treated effectively as two-electron systems with efficient non-empirical pseudopotentials in their semi-local form [77] used to replace core electrons. Additionally to the pseudopotential treatment, the self-consistent field (SCF) computations are followed by a full valence configuration interaction (FCI) calculations using the CIPSI algorithm (Configuration Interaction by Perturbation of a multiconfiguration wave function Selected Iteratively) of the standard succession of programs developed by the ‘Laboratoire de Chimie et Physique de Toulouse’. The core-valence electronic correlations between the polarizable Ca²⁺ and Alk⁺ cores with the valence electrons are included by using core polarization potentials (CPP) [78].

Valence electrons are described with large Gaussian basis sets. For Ca the (8s, 7p, 7d)/[8s, 7p, 5d] basis set developed in reference [73] together with the corresponding s, p, and d cut-off parameters of the pseudopotential ($\rho_s^{\text{Ca}^+} = 1.77405$, $\rho_p^{\text{Ca}^+} = 1.81$, $\rho_d^{\text{Ca}^+} = 1.691$) optimized in order to reproduce the ionization energy of the Ca⁺ ion are employed. For Li, Na, K, Rb, and Cs, respectively, the (9s, 8p, 6d)/[8s, 6p, 5d], (7s, 6p, 5d)/[6s, 5p, 4d], (8s, 6p, 3d)/[8s, 5p, 5d], (7s, 4p, 5d)/[6s, 4p, 4d], and (7s, 4p, 5d)/[6s, 4p, 4d] basis sets are used together with the following cut-off parameters ($\rho_s^{\text{Li}} = 1.434$, $\rho_p^{\text{Li}} = 0.982$, $\rho_d^{\text{Li}} = 0.6$), ($\rho_s^{\text{Na}} = 1.4423$, $\rho_p^{\text{Na}} = 1.625$, $\rho_d^{\text{Na}} = 1.5$), ($\rho_s^{\text{K}} = 2.115$, $\rho_p^{\text{K}} = 2.1125$, $\rho_d^{\text{K}} = 1.983$), ($\rho_s^{\text{Rb}} = 2.5213$, $\rho_p^{\text{Rb}} = 2.2790$, $\rho_d^{\text{Rb}} = 2.5110$), ($\rho_s^{\text{Cs}} = 2.690$, $\rho_p^{\text{Cs}} = 1.850$, $\rho_d^{\text{Cs}} = 2.810$) [64–71]. The core

Table 1. Lowest atomic asymptotes, their experimental E_{Exp} and calculated E_{Th} valence energies, and associated molecular electronic states of the CaAlk^+ (Alk = Li, Na, K, Rb, Cs) molecular ions. Experimental energies are averaged on spin-orbit manifold if appropriate. $\Delta E = E_{\text{Th}} - E_{\text{Exp}}$.

Asymptote	Molecular states	E_{Exp} (cm^{-1}) [80]	E_{Th} (cm^{-1})	$ \Delta E $ (cm^{-1})
CaLi⁺				
$\text{Ca}(^1\text{S}) + \text{Li}^+(^1\text{S})$	$^1\Sigma^+$	-145 058	-144 904	154
$\text{Ca}^+(^2\text{S}) + \text{Li}(^2\text{S})$	$^1\Sigma^+, ^3\Sigma^+$	-139 239	-139 240	1
$\text{Ca}(^3\text{P}) + \text{Li}^+(^1\text{S})$	$^3\Sigma^+, ^3\Pi$	-129 795	-129 624	171
$\text{Ca}^+(^2\text{D}) + \text{Li}(^2\text{S})$	$^1\Sigma^+, ^3\Sigma^+, ^1\Pi, ^3\Pi, ^1\Delta, ^3\Delta$	-125 550	-125 592	42
$\text{Ca}(^3\text{D}) + \text{Li}^+(^1\text{S})$	$^3\Sigma^+, ^3\Pi, ^3\Delta$	-124 702	-124 136	566
$\text{Ca}^+(^2\text{S}) + \text{Li}(^2\text{P})$	$^1\Sigma^+, ^3\Sigma^+, ^1\Pi, ^3\Pi$	-124 232	-124 337	105
$\text{Ca}(^1\text{D}) + \text{Li}^+(^1\text{S})$	$^1\Sigma^+, ^1\Pi, ^1\Delta$	-123 208	-122 611	597
CaNa⁺				
$\text{Ca}(^1\text{S}) + \text{Na}^+(^1\text{S})$	$^1\Sigma^+$	-145 058	-144 904	154
$\text{Ca}^+(^2\text{S}) + \text{Na}(^2\text{S})$	$^1\Sigma^+, ^3\Sigma^+$	-137 201	-137 203	2
$\text{Ca}(^3\text{P}) + \text{Na}^+(^1\text{S})$	$^3\Sigma^+, ^3\Pi$	-129 795	-129 624	171
$\text{Ca}(^3\text{D}) + \text{Na}^+(^1\text{S})$	$^3\Sigma^+, ^3\Pi, ^3\Delta$	-124 702	-124 136	566
$\text{Ca}^+(^2\text{D}) + \text{Na}(^2\text{S})$	$^1\Sigma^+, ^3\Sigma^+, ^1\Pi, ^3\Pi, ^1\Delta, ^3\Delta$	-123 514	-123 554	40
$\text{Ca}(^1\text{D}) + \text{Na}^+(^1\text{S})$	$^1\Sigma^+, ^1\Pi, ^1\Delta$	-123 208	-122 611	597
$\text{Ca}(^1\text{P}) + \text{Na}^+(^1\text{S})$	$^1\Sigma^+, ^1\Pi$	-121 405	-121 574	169
CaK⁺				
$\text{Ca}(^1\text{S}) + \text{K}^+(^1\text{S})$	$^1\Sigma^+$	-145 058	-144 904	154
$\text{Ca}^+(^2\text{S}) + \text{K}(^2\text{S})$	$^1\Sigma^+, ^3\Sigma^+$	-130 760	-130 763	3
$\text{Ca}(^3\text{P}) + \text{K}^+(^1\text{S})$	$^3\Sigma^+, ^3\Pi$	-129 795	-129 624	171
$\text{Ca}(^3\text{D}) + \text{K}^+(^1\text{S})$	$^3\Sigma^+, ^3\Pi, ^3\Delta$	-124 702	-124 136	566
$\text{Ca}(^1\text{D}) + \text{K}^+(^1\text{S})$	$^1\Sigma^+, ^1\Pi, ^1\Delta$	-123 208	-122 611	597
$\text{Ca}(^1\text{P}) + \text{K}^+(^1\text{S})$	$^1\Sigma^+, ^1\Pi$	-121 405	-121 574	169
$\text{Ca}^+(^2\text{S}) + \text{K}(^2\text{P})$	$^1\Sigma^+, ^3\Sigma^+, ^1\Pi, ^3\Pi$	-117 739	-117 757	18
CaRb⁺				
$\text{Ca}(^1\text{S}) + \text{Rb}^+(^1\text{S})$	$^1\Sigma^+$	-145 058	-144 904	154
$\text{Ca}(^3\text{P}) + \text{Rb}^+(^1\text{S})$	$^3\Sigma^+, ^3\Pi$	-129 795	-129 624	171
$\text{Ca}^+(^2\text{S}) + \text{Rb}(^2\text{S})$	$^1\Sigma^+, ^3\Sigma^+$	-129 443	-129 445	2
$\text{Ca}(^3\text{D}) + \text{Rb}^+(^1\text{S})$	$^3\Sigma^+, ^3\Pi, ^3\Delta$	-124 702	-124 136	566
$\text{Ca}(^1\text{D}) + \text{Rb}^+(^1\text{S})$	$^1\Sigma^+, ^1\Pi, ^1\Delta$	-123 208	-122 611	597
$\text{Ca}(^1\text{P}) + \text{Rb}^+(^1\text{S})$	$^1\Sigma^+, ^1\Pi$	-121 405	-121 574	169
$\text{Ca}^+(^2\text{S}) + \text{Rb}(^2\text{P})$	$^1\Sigma^+, ^3\Sigma^+, ^1\Pi, ^3\Pi$	-116 705	-116 724	19
CaCs⁺				
$\text{Ca}(^1\text{S}) + \text{Cs}^+(^1\text{S})$	$^1\Sigma^+$	-145 058	-144 904	154
$\text{Ca}(^3\text{P}) + \text{Cs}^+(^1\text{S})$	$^3\Sigma^+, ^3\Pi$	-129 795	-129 624	171
$\text{Ca}^+(^2\text{S}) + \text{Cs}(^2\text{S})$	$^1\Sigma^+, ^3\Sigma^+$	-127 158	-127 163	5
$\text{Ca}(^3\text{D}) + \text{Cs}^+(^1\text{S})$	$^3\Sigma^+, ^3\Pi, ^3\Delta$	-124 702	-124 136	566
$\text{Ca}(^1\text{D}) + \text{Cs}^+(^1\text{S})$	$^1\Sigma^+, ^1\Pi, ^1\Delta$	-123 208	-122 611	597
$\text{Ca}(^1\text{P}) + \text{Cs}^+(^1\text{S})$	$^1\Sigma^+, ^1\Pi$	-121 405	-121 574	169
$\text{Ca}^+(^2\text{S}) + \text{Cs}(^2\text{P})$	$^1\Sigma^+, ^3\Sigma^+, ^1\Pi, ^3\Pi$	-115 611	-115 619	8

polarizabilities of the Ca^+ ion and alkali atoms are taken to be $\alpha^{\text{Ca}^{2+}} = 3.1717 a_0^3$, $\alpha^{\text{Li}^+} = 0.1917 a_0^3$, $\alpha^{\text{Na}^+} = 0.9930 a_0^3$, $\alpha^{\text{K}^+} = 5.457 a_0^3$, $\alpha^{\text{Rb}^+} = 9.245 a_0^3$ and $\alpha^{\text{Cs}^+} = 15.117 a_0^3$ [64–71, 73, 79]. Employed models reproduce atomic properties with good accuracy when compared with previous theoretical results and experimental measurements [64–71].

In the present work, the interaction of the considered alkali-metal and alkaline-earth-metal atoms and ions in the ground and different excited electronic states results in different molecular electronic states of the singlet or triplet Σ^+ , Π , and Δ symmetries. The lowest seven atomic thresholds for each of the considered CaAlk^+ molecular ions, together with their valence energies (i.e., binding energies of valence electrons) and associated molecular electronic states, are collected in table 1. The binding energy of valence electrons is the difference between the energy of the $(\text{Ca} + \text{Alk})^+$ atomic threshold in a given electronic state with two valence electrons and the $(\text{Ca} + \text{Alk})^{3+}$ triple ionized form without any valence electrons of Ca or Alk. Experimental values are obtained from the first and second ionization energies of Ca and the first ionization energy of Alk [80]. The same values repeat for atomic thresholds with an ionized alkali-metal atom $\text{Ca} + \text{Alk}^+$, where Alk^+ does not have any valence electron, and it does not contribute to the considered valence energy. Thus, repeating numbers represent the accuracy of energies of Ca. The calculated energies of $\text{Ca}^+(^2\text{S}) + \text{Alk}(^2\text{S})$ limits, which describe essential ground-state collisions of alkaline-earth-metal ions with alkali-metal atoms, agree very well (within 5 cm^{-1}) with experimental

values. Description of the 1D and 3D excited electronic states of the Ca atom is the most challenging with discrepancies of 597 cm^{-1} and 566 cm^{-1} for related atomic limits, respectively. Nevertheless, the overall agreement is good, suggesting good accuracy of molecular calculations.

The spectroscopic constants are extracted from the *ab initio* points interpolated using the cubic spline method. The permanent and transition electric dipole moments are calculated as expectation values of the dipole operator with the calculated electronic wavefunctions. The z axis is chosen along the internuclear axis and is oriented from a Ca atom to an alkali-metal atom. The origin is set in the center of mass. Masses of the most abundant isotopes are assumed within the paper.

The time-independent Schrödinger equation for the nuclear motion is solved using the renormalized Numerov algorithm with step-size doubling and about 100 step points per de Broglie wavelength [81] for both bound [64] and continuum states [34]. Rate constants for elastic scattering and inelastic charge-exchange reactive collisions are calculated as implemented and described in references [34, 82]. The wave functions are propagated from small finite interatomic separations in the classically forbidden region where the scattering wave-function amplitude is negligible to large interatomic separations where electronic potentials are negligible as compared to the collision energy. Then, the K and S matrices are extracted by imposing the long-range scattering boundary conditions in terms of the Bessel functions. The elastic rate constants and scattering lengths are obtained from the S matrix for the entrance channel, while inelastic rate constants are computed using the Fermi golden rule type expressions based on the Einstein coefficients between bound and continuum nuclear wave functions of relevant electronic states.

The radiative lifetimes τ_v of vibrational levels v , $\tau_v = 1/\Gamma_v$, are calculated from the radiative rates $\Gamma_v = \sum_{v' < v} A_{vv'} + \sum_{v'} B_{vv'}$, which are given by the sums of the Einstein coefficients for the spontaneous emission $A_{vv'}$ and coefficients for the absorption and stimulated emission $B_{vv'}$. The coefficients for the spontaneous emission $A_{vv'} \sim \omega_{vv'}^3 d_{vv'}^2$ are proportional to the third power of the transition frequencies $\omega_{vv'}$ and second power of the transition dipole moments $d_{vv'}$ between the initial v and the final v' vibrational states. The coefficients for the absorption and stimulated emission are proportional to the coefficients for the spontaneous emission and the spectral energy density of the present black body radiation [83, 84]. The bound-continuum transitions are included either using the Franck–Condon approximation [83] or the sum rule approximation [85], and both methods give the same results.

3. Results and discussion

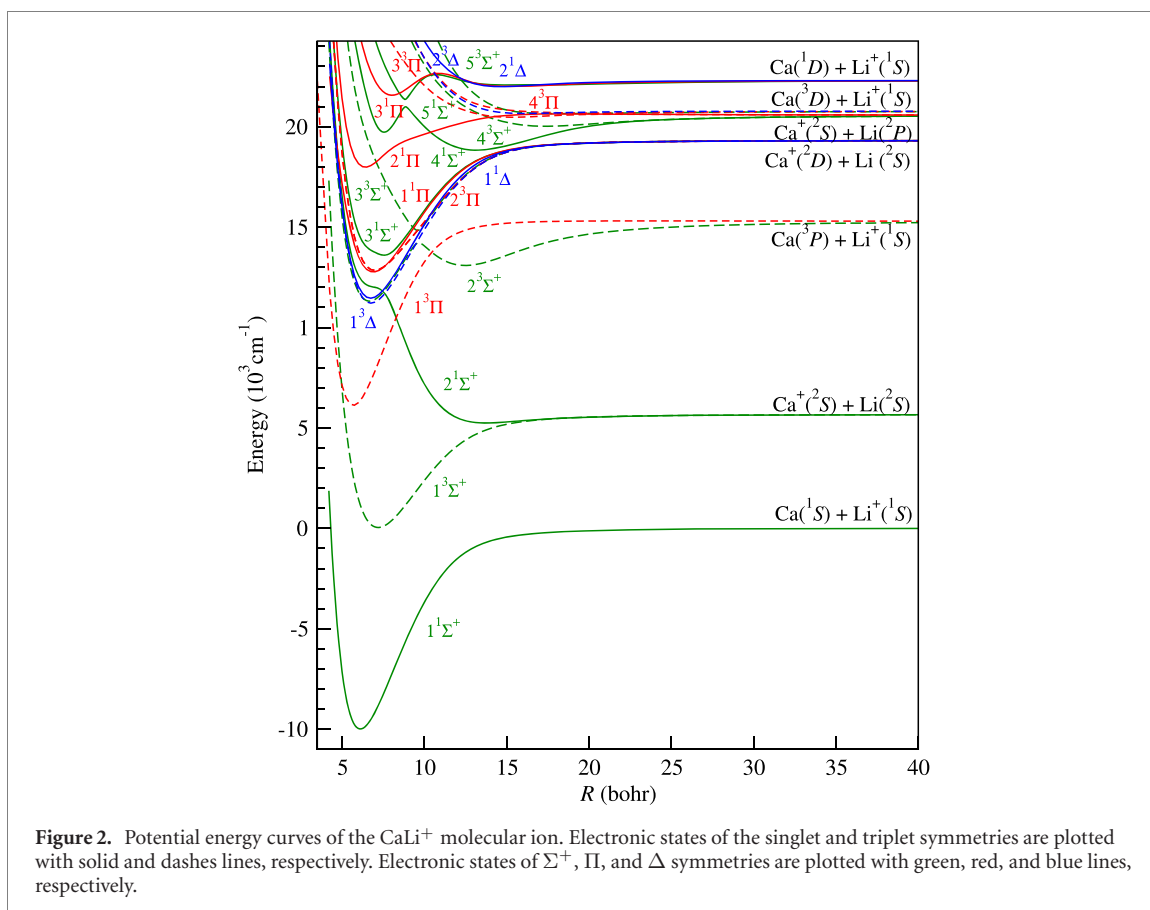
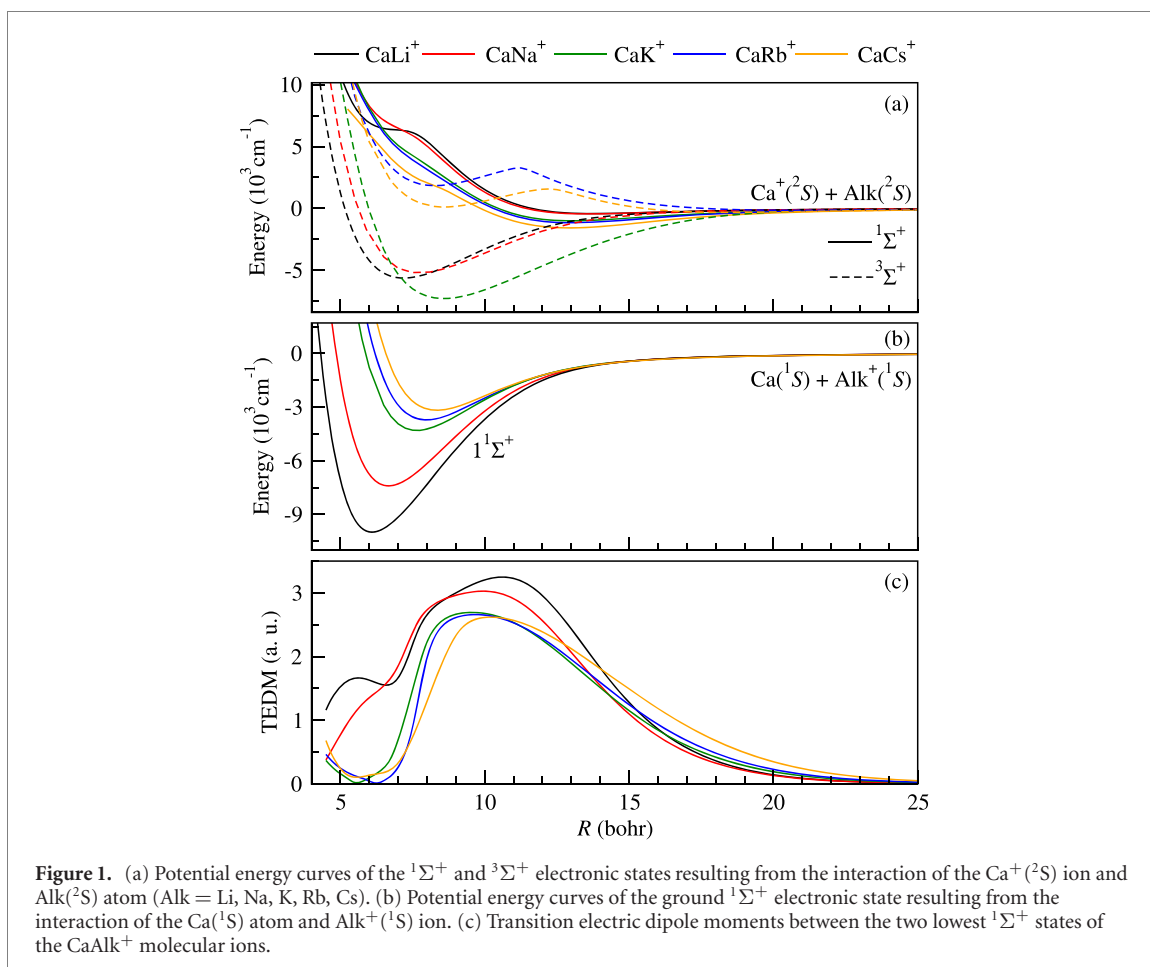
3.1. Potential energy curves

Potential energy curves (PECs) for the ground and several excited electronic states of the CaLi^+ , CaNa^+ , CaK^+ , CaRb^+ , and CaCs^+ molecular ions are presented in figures 1–6. All electronic states correlated with the seven lowest atomic thresholds of each system are investigated (see table 1). Thus, several singlet and triplet electronic states of the Σ^+ , Π , and Δ spatial symmetries are studied. Spectroscopic characteristics of calculated PECs, i.e. equilibrium interatomic distances R_e , well depths D_e , transition energies T_e , harmonic constants ω_e , anharmonicity constants $\omega_e x_e$, and rotational constants B_e , are collected in tables 2–6. Results for excited states of the CaK^+ and CaCs^+ molecular ions are reported for the first time, while spectroscopic constants for other systems are compared with previous available results.

Interactions between the ground-state Ca^+ ion and ground-state alkali-metal atom are described by the $^1\Sigma^+$ and $^3\Sigma^+$ electronic states and govern ground-state collisions in respective hybrid ion–atom experiments [1]. For all considered mixtures, these states are electronically excited, and the radiative charge-transfer and association processes are energetically allowed and may lead to collisional losses [82] leading to the $^1\Sigma^+$ ground electronic state. Therefore in figure 1, we present and compare electronic states correlated with $\text{Ca}^+(^2S) + \text{Alk}(^2S)$ and $\text{Ca}(^1S) + \text{Alk}^+(^1S)$ atomic thresholds, and transition electric dipole moments between the two lowest $^1\Sigma^+$ electronic states, which drive radiative losses. Corresponding rate constants for reactive collisions are presented in section 3.4.

The ground-state properties of the CaAlk^+ molecular ions are similar to those predicted for the SrAlk^+ systems [76]. The $^1\Sigma^+$ ground electronic state dissociate into $\text{Ca}(^1S) + \text{Alk}^+(^1S)$. Therefore, its long-range behavior is very similar for all considered molecular ions and is determined by the induction interaction of the charge of the alkali-metal ion with the polarizability of the Ca atom (see figure 1(b)). The short-range behavior depends more on the involved alkali-metal ion and have covalent bonding nature. The well depth decreases with the mass of the alkali-metal ion from 9986 cm^{-1} for CaLi^+ to 3174 cm^{-1} for CaCs^+ , while the equilibrium distance increases with the mass of the alkali-metal ion from 6.11 bohr for CaLi^+ to 8.34 bohr for CaCs^+ .

The presented ground-state PECs can be compared with recent results calculated with the small-core pseudopotentials and coupled cluster method [53]. The well depths obtained with the two methods agree



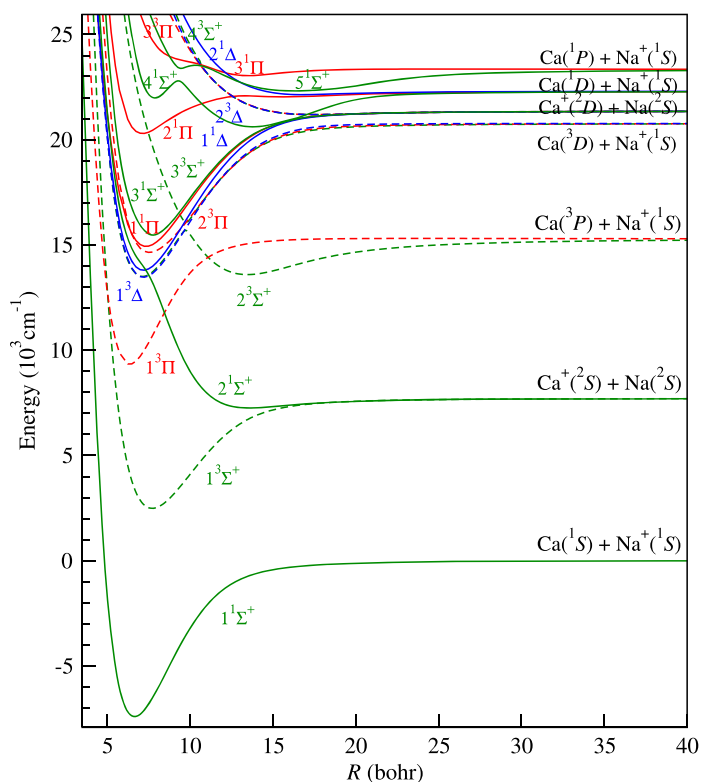


Figure 3. Potential energy curves of the CaNa^+ molecular ion. Line styles are used as described in figure 2.

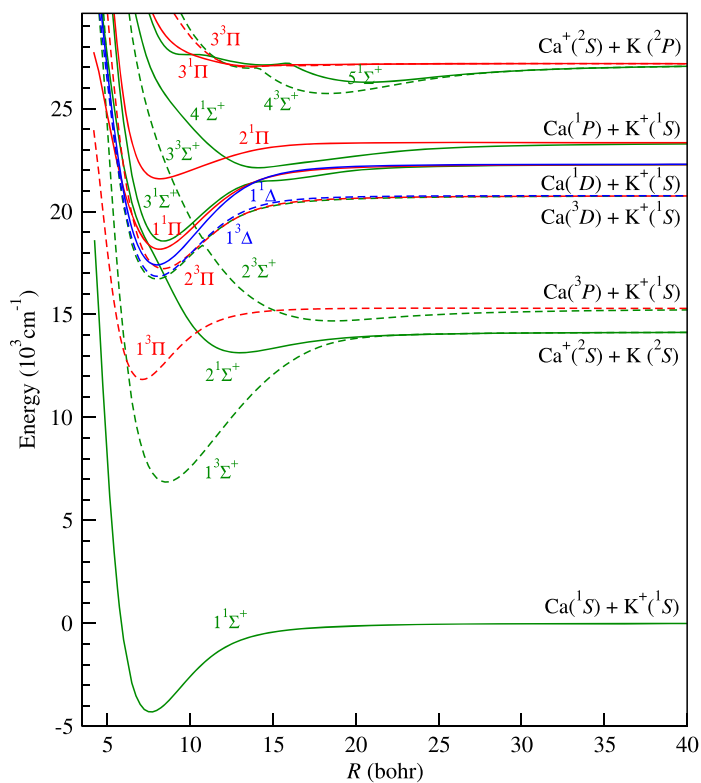


Figure 4. Potential energy curves of the CaK^+ molecular ion. Line styles are used as described in figure 2.

with the mean absolute difference of 68 cm^{-1} (1.7%), while the equilibrium distances agree with the mean difference of 0.084 bohr (1.1%). Calculations with large-core pseudopotentials give slightly smaller equilibrium distances and deeper well depths, but the overall good agreement cross validates both

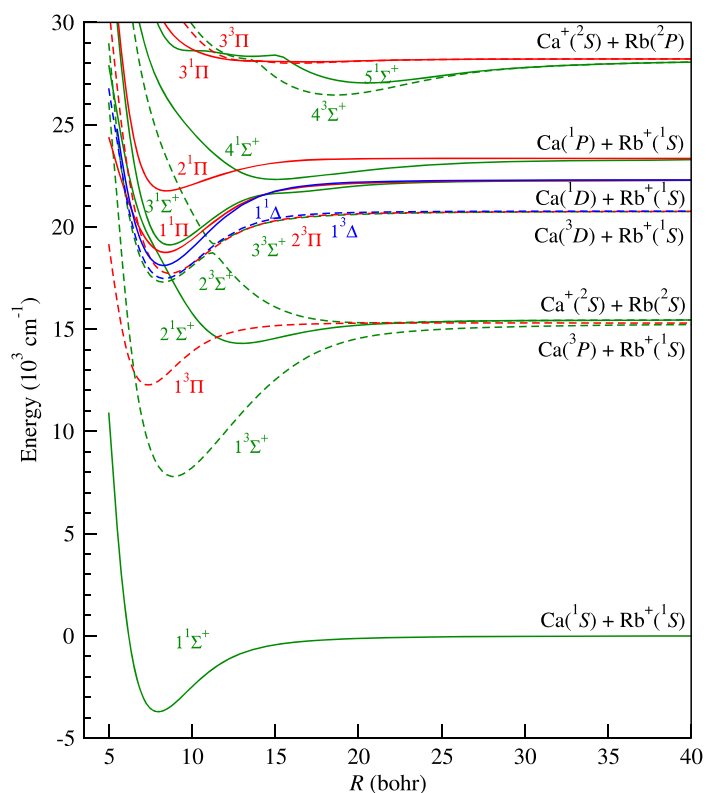


Figure 5. Potential energy curves of the CaRb^+ molecular ion. Line styles are used as described in figure 2.

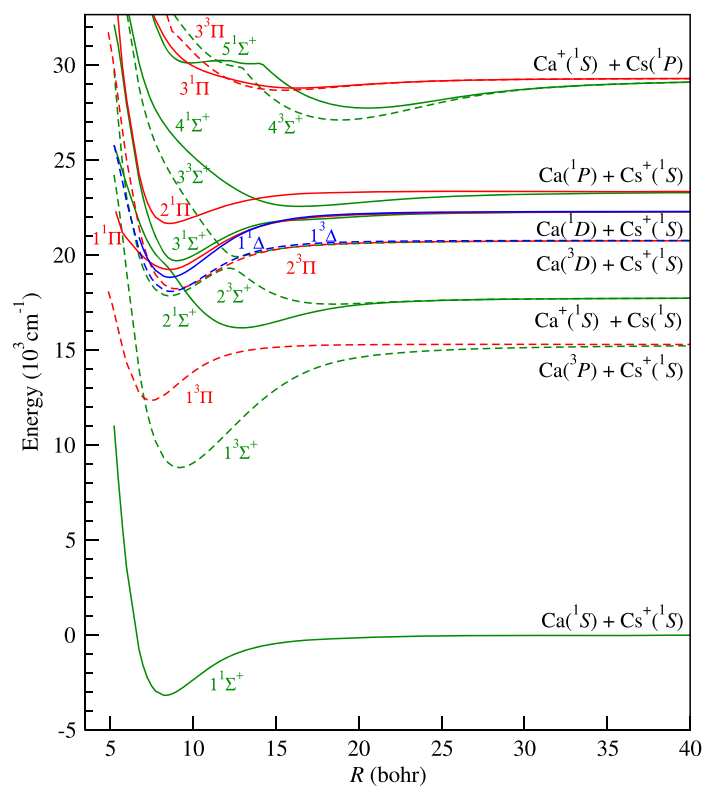


Figure 6. Potential energy curves of the CaCs^+ molecular ion. Line styles are used as described in figure 2.

approaches and suggests that similar accuracy may be expected for excited electronic states. The agreement with older results collected in tables 2–6 is also satisfactory.

Table 2. Spectroscopic constants of the ground and excited electronic states of the CaLi⁺ molecular ion.

State	R_e (bohr)	D_e (cm ⁻¹)	T_e (cm ⁻¹)	ω_e (cm ⁻¹)	$\omega_e x_e$ (cm ⁻¹)	B_e (cm ⁻¹)	References
1 ¹ Σ ⁺	6.11	9986	0	244.19	1.49	0.272 557	This work
	6.16	9941	0	246	—	0.266	[53]
	6.165	10 093	0	245.1	1.31	0.2650	[54]
	6.120	9973	0	242	—	—	[55]
	6.210	9641	0	—	—	—	[56]
	6.273	9990	0	242	—	—	[57]
2 ¹ Σ ⁺	6.200	8943	0	235	—	—	[58]
	13.74	411	15 237	44.03	1.17	0.053 897	This work
	22.41	23	16 500	6.5	0.63	0.0201	[54]
3 ¹ Σ ⁺	13.68	412	—	41	—	—	[55]
	7.56	5705	23 592	154.27	1.04	0.178 031	This work
4 ¹ Σ ⁺	7.42	5816	—	132	—	—	[55]
	7.55	1262	29 719	247.15	19.09	0.178 503	This work
2nd min	7.51	1192	—	—	—	—	[55]
	13.16	1741	28 820	61.82	0.71	0.058 753	This work
5 ¹ Σ ⁺	13.22	1975	—	—	—	—	[55]
	8.82	1235	31 379	370.31	34.95	0.130 799	This work
2nd min	15.00	200	32 070	22.13	0.61	0.045 223	This work
1 ³ Σ ⁺	7.19	5616	10 033	163.19	1.19	0.196 826	This work
	7.18	5792	—	—	—	—	[55]
2 ³ Σ ⁺	6.66	3911	21 305	185.17	2.19	0.229 399	This work
	6.69	3693	—	—	—	—	[55]
2nd min	12.49	2132	23 084	72.11	0.61	0.065 255	This work
	12.53	1807	—	—	—	—	[55]
3 ³ Σ ⁺	9.56	4456	24 843	287.35	4.63	0.111 333	This work
	9.54	4514	—	—	—	—	[55]
4 ³ Σ ⁺	17.37	503	30 016	32.91	0.54	0.033 724	This work
	16.89	325	—	—	—	—	[55]
5 ³ Σ ⁺	18.33	109	30 645	14	0.45	0.030 284	This work
1 ¹ Π	6.90	6541	22 757	172.23	1.13	0.213 718	This work
	6.472	1372	34 548	214.8	1.66	0.2397	[54]
	6.69	6643	—	—	—	—	[55]
2 ¹ Π	6.41	2599	27 976	184.20	3.26	0.247 642	This work
	6.43	2939	—	—	—	—	[55]
3 ¹ Π	8.04	715	31 560	149.74	7.84	0.157 408	This work
	8.18	502	—	—	—	—	[55]
2nd min	15.18	280	31 994	31.87	0.91	0.044 157	This work
	16.1	162	—	—	—	—	[55]
1 ³ Π	5.69	9172	16 116	255.88	1.78	0.314 279	This work
	5.879	7621	19 933	255.9	1.57	0.2904	[54]
	5.71	8982	—	—	—	—	[55]
2 ³ Π	6.98	6460	22 837	168.61	1.10	0.208 847	This work
	6.87	6686	—	—	—	—	[55]
3 ³ Π	15.32	110	30 465	31.94	2.32	0.043 353	This work
1 ¹ Δ	6.73	7854	21 452	186.25	1.10	0.224 652	This work
	6.71	7959	—	—	—	—	[55]
2 ¹ Δ	14.63	298	31 988	37.98	1.21	0.047 539	This work
1 ³ Δ	6.75	8097	21 207	187.75	1.09	0.223 322	This work
	6.73	8212	—	—	—	—	[55]
2 ³ Δ	16.10	108	30 653	24.11	1.35	0.039 254	This work

The energy difference between the lowest Ca(¹S) + Alk(¹S) and Ca⁺(²S) + Alk(²S) dissociation thresholds increases with the mass of alkali-metal atom from 5819 cm⁻¹ for CaLi⁺ to 17 880 cm⁻¹ for CaCs⁺. The well depth of the 2¹Σ⁺ state dissociating into Ca⁺(²S) + Alk(²S) increases with the mass of alkali-metal atom from 411 cm⁻¹ for CaLi⁺ to 1574 cm⁻¹ for CaCs⁺, while the equilibrium distance decreases slightly from 13.74 bohr for CaLi⁺ to 12.92 bohr for CaCs⁺. The 2¹Σ⁺ electronic state is relatively shallow because of its non-bonding nature around the equilibrium distance and avoided crossing with the ground 1¹Σ⁺ electronic state. The 3¹Σ⁺ electronic state associated with the Ca⁺(²S) + Alk(²S) atomic threshold is the lowest triplet state for the CaLi⁺, CaNa⁺, and CaK⁺ molecular ions, while it is the first excited triplet state for the CaRb⁺ and CaCs⁺ molecular ions. The change of the order of the Ca⁺(²S) + Alk(²S) and Ca(³P) + Alk(¹S) atomic thresholds in CaRb⁺ and CaCs⁺ visibly affects their 3¹Σ⁺ electronic states dissociating into Ca⁺(²S) + Alk(²S), which are much shallower because of avoided crossing with lower lying 3³Σ⁺ states (see figure 1(a)). Thus, no clear trend is observed for the lowest 3¹Σ⁺ electronic states. For example, the well depth and equilibrium distance of the first 3¹Σ⁺ state in CaK⁺ is 7275 cm⁻¹ and 8.58 bohr, respectively.

Table 3. Spectroscopic constants of the ground and excited electronic states of the CaNa⁺ molecular ion.

State	R_e (bohr)	D_e (cm ⁻¹)	T_e (cm ⁻¹)	ω_e (cm ⁻¹)	$\omega_e x_e$ (cm ⁻¹)	B_e (cm ⁻¹)	References
$1^1\Sigma^+$	6.67	7402	0	135.79	0.62	0.092 621	This work
	6.70	7336	0	137	—	0.0918	[53]
	6.67	7441	0	141.84	0.674	0.0926	[60]
	6.67	7488	0	138.43	0.58	0.093 413	[59]
	6.76	6376	0	—	—	—	[10]
$2^1\Sigma^+$	13.59	443	14 660	30.02	0.51	0.022 311	This work
	13.57	446	—	27.30	0.432	0.0223	[60]
	13.44	450	15 069	29.86	0.55	0.022 822	[59]
$3^1\Sigma^+$	7.77	5869	22 873	110.07	0.52	0.068 253	This work
	7.77	6007	—	102.72	0.438	0.0582	[60]
	7.76	6311	23 026	102.59	0.43	0.069 019	[59]
$4^1\Sigma^+$	7.88	792	29 387	132.70	14.62	0.066 361	This work
	7.95	1107	28 339	164.03	1.87	0.029 906	[59]
2nd min	13.73	1686	28 011	42.81	0.28	0.021 861	This work
$5^1\Sigma^+$	13.23	1203	28 243	48.98	1.87	0.029 906	[59]
	16.37	1018	29 718	20.34	0.10	0.015 581	This work
$1^3\Sigma^+$	7.73	5210	9891	97.98	0.46	0.068 961	This work
	7.72	5345	—	107.7	0.532	0.0691	[60]
$2^3\Sigma^+$	7.15	1738	20 906	109.97	1.74	0.080 603	This work
	7.17	1578	—	26.67	0.112	0.0801	[60]
2nd min	13.48	1650	20 994	40.71	0.25	0.022 677	This work
$3^3\Sigma^+$	13.53	1719	—	30.64	0.135	0.0225	[60]
	9.77	4688	23 471	156.42	1.30	0.043 169	This work
$4^3\Sigma^+$	9.75	4426	—	120.10	0.79	0.0433	[60]
	17.66	153	28 597	12.96	0.27	0.013 212	This work
$1^1\Pi$	16.55	191	—	11.80	0.173	0.0150	[60]
	7.36	6415	22 335	101.36	0.4	0.076 069	This work
$2^1\Pi$	7.37	6608	—	105.80	0.418	0.0758	[60]
	7.32	6928	22 352	103.04	0.38	0.077 102	[59]
	7.14	1994	27 697	95.76	1.15	0.080 829	This work
$2^3\Pi$	7.15	2111	—	78.43	0.691	0.806	[60]
	7.10	2100	27 367	103.56	1.00	0.082 348	[59]
	15.65	256	29 435	17.55	0.30	0.016 824	This work
$3^1\Pi$	16.40	248	—	13.58	0.254	0.0153	[60]
	13.47	301	30 446	31.73	0.84	0.022 711	This work
$1^3\Pi$	13.78	259	—	28.83	0.730	0.0217	[60]
	6.36	5964	16 733	139.08	0.81	0.101 870	This work
$2^3\Pi$	6.39	5930	—	144.50	0.861	0.1009	[60]
	7.56	6115	22 048	94.01	0.36	0.072 097	This work
$3^3\Pi$	7.54	5895	—	101.40	0.43	0.0724	[60]
	17.48	154	28 597	14.33	0.33	0.013 486	This work
$1^1\Delta$	16.57	191	—	14.75	0.286	0.0150	[60]
	7.19	7552	21 200	109.13	0.39	0.079 708	This work
$2^1\Delta$	7.19	7706	—	111.91	0.40	0.0797	[60]
	16.81	156	29 544	16.40	0.43	0.014 582	This work
$1^3\Delta$	17.74	104	—	13.29	0.43	0.0131	[60]
	7.20	7302	20 870	108.91	0.41	0.079 487	This work
$2^3\Delta$	7.20	7063	—	111.32	0.410	0.0794	[60]
	17.66	155	28 597	13.63	0.30	0.013 212	This work
	16.73	196	—	15.24	0.299	0.0147	[60]

The density of electronic states increases with the excitation energy, and for all investigated molecular ions, several avoided crossings between excited states of the same electronic symmetry can be found. Strong radial non-adiabatic couplings between involved electronic states can be expected. Some of the excited atomic thresholds are close together that furthermore facilitates interactions between associated electronic states. As a result, several excited states have double-well structures. For example, all $2^3\Sigma^+$ states are significantly repulsive at the short-range distances, partially due to broad avoided crossing with $1^3\Sigma^+$ states, and thus they intersect with attractive $3^3\Sigma^+$ states, forming narrow avoided crossings at the short range. Avoided crossings between $2^1\Sigma^+$, $3^1\Sigma^+$, and $4^1\Sigma^+$ at short- and intermediate-range distances are also pronounced. Additionally, electronic states of different spin and spatial symmetries intersect with each other. These crossings may become avoided crossings if relativistic spin-orbit couplings would be included, which is out of the scope of this paper. Avoided and real crossings may provide mechanism for efficient non-radiative and non-adiabatic charge transfer between ions and atoms in excited electronic states [23, 61, 86, 87].

Table 4. Spectroscopic constants of the ground and excited electronic states of the CaK⁺ molecular ion.

State	R_e (bohr)	D_e (cm ⁻¹)	T_e (cm ⁻¹)	ω_e (cm ⁻¹)	$\omega_e x_e$ (cm ⁻¹)	B_e (cm ⁻¹)	References
1 ¹ Σ ⁺	7.65	4306	0	92.60	0.49	0.052 002	This work
	7.71	4281	0	93.2	—	0.0513	[53]
2 ¹ Σ ⁺	13.02	992	17 451	33.11	0.27	0.017 953	This work
3 ¹ Σ ⁺	8.40	3718	22 874	78.32	0.41	0.043 131	This work
4 ¹ Σ ⁺	14.10	1177	26 434	35.18	0.26	0.015 308	This work
5 ¹ Σ ⁺	20.68	809	30 590	18.18	0.10	0.007 12	This work
1 ³ Σ ⁺	8.58	7275	11 169	78.10	0.21	0.041 340	This work
2 ³ Σ ⁺	18.66	559	18 999	18.37	0.15	0.008 740	This work
2nd min	8.02	-1471	21 029	76.95	1.01	0.047 315	This work
3 ³ Σ ⁺	10.89	2086	22 980	163.59	3.21	0.025 662	This work
4 ³ Σ ⁺	18.30	1366	30 044	23.35	0.10	0.009 088	This work
1 ¹ Π	8.17	4116	22 482	72.24	0.32	0.045 594	This work
2 ¹ Π	8.20	1751	25 900	56.42	0.45	0.045 261	This work
3 ¹ Π	13.86	111	31 365	21.27	1.02	0.015 842	This work
1 ³ Π	7.14	3446	16 148	94.98	0.65	0.059 697	This work
2 ³ Π	8.39	3539	21 529	71.99	0.37	0.043 234	This work
3 ³ Π	13.57	152	31 317	35.31	2.05	0.016 527	This work
1 ¹ Δ	8.01	4887	21 718	79.32	0.32	0.047 433	This work
1 ³ Δ	8.06	3918	21 160	77.20	0.38	0.046 847	This work

Table 5. Spectroscopic constants of the ground and excited electronic states of the CaRb⁺ molecular ion.

State	R_e (bohr)	D_e (cm ⁻¹)	T_e (cm ⁻¹)	ω_e (cm ⁻¹)	$\omega_e x_e$ (cm ⁻¹)	B_e (cm ⁻¹)	References
1 ¹ Σ ⁺	7.97	3714	0	73.53	0.35	0.034 735	This work
	8.06	3666	0	73.9	—	0.0341	[53]
	7.96	3851	0	73.02	—	0.034 60	[35]
	8.26	3717	0	73.43	0.50	0.032 371	[62]
	8.0	3730	0	—	—	—	[61]
2 ¹ Σ ⁺	12.99	1160	18 015	29.58	0.15	0.013 076	This work
	12.82	1284	17 764	28.20	0.09	0.013 388	[62]
	12.86	1272	18 171	29.89	—	0.013 30	[35]
	13	1170	—	—	—	—	[61]
3 ¹ Σ ⁺	8.65	3175	22 835	62.04	0.34	0.029 489	This work
4 ¹ Σ ⁺	14.89	1016	26 035	22.61	0.31	0.009 952	This work
5 ¹ Σ ⁺	13.61	2051	30 754	16.9	0.31	0.011 912	This work
1 ³ Σ ⁺	8.90	7494	11 503	64.21	0.16	0.027 855	This work
	9.15	7455	10 806	77.92	0.20	0.026 367	[62]
2 ³ Σ ⁺	8.27	-1839	21 014	61.54	0.49	0.032 261	This work
	8.31	-1496	20 128	—	—	0.031 976	[62]
2nd min	20.82	137	19 025	8.37	0.13	0.005 090	This work
	17.82	121	19 018	—	—	—	[62]
3 ³ Σ ⁺	11.42	1481	22 999	61.54	0.49	0.016 918	This work
4 ³ Σ ⁺	18.57	1745	30 163	20.67	0.04	0.006 398	This work
1 ¹ Π	8.43	3542	22 467	57.48	0.16	0.031 048	This work
2 ¹ Π	8.47	1575	25 476	46.14	0.51	0.030 755	This work
3 ¹ Π	17.0	131	31 782	8.70	0.07	0.007 635	This work
1 ³ Π	7.38	3022	15 982	75.86	0.40	0.040 511	This work
	7.63	3308	18 204	—	—	—	[62]
2 ³ Π	8.67	3037	21 440	58.30	0.21	0.029 353	This work
3 ³ Π	16.19	202	31 718	12.17	0.16	0.008 418	This work
1 ¹ Δ	8.29	4184	21 827	63.51	0.18	0.032 105	This work
1 ³ Δ	8.35	3293	21 189	61.17	0.24	0.031 646	This work

Spectroscopic constants of calculated excited electronic states for the investigated molecular ions are collected in tables 2–6. Results for excited electronic states of the CaK⁺ and CaCs⁺ molecular ions are reported for the first time, while spectroscopic constants for other systems can be compared with previous available theoretical results [10, 15, 35, 53–62]. Similarly as for the ground electronic state, the results for the excited states obtained with different computational methods agree reasonably well. Both well depths and equilibrium distances mostly agree within several percent. In the case of the CaLi⁺ molecular ion, the present results agree very well with the results of references [15, 55], while well depths seem to be underestimated in calculations presented in reference [54], which employed a single-reference method. For the CaNa⁺ molecular ion, the present results agree very well with the results of references [59, 60], while the agreement is worse with calculations presented in reference [10], which employed smaller basis sets. In the

Table 6. Spectroscopic constants of the ground and excited electronic states of CaCs^+ molecular ion.

State	R_e (bohr)	D_e (cm^{-1})	T_e (cm^{-1})	ω_e (cm^{-1})	$\omega_e x_e$ (cm^{-1})	B_e (cm^{-1})	References
$1^1\Sigma^+$	8.34	3174	0	64.78	0.33	0.028 107	This work
	8.53	3017	0	63.2	—	0.0270	[53]
$2^1\Sigma^+$	12.92	1574	19 344	29.78	0.14	0.011 712	This work
$3^1\Sigma^+$	9.02	2584	22 877	59.85	0.35	0.024 029	This work
$4^1\Sigma^+$	16.45	772	25 739	15.67	0.08	0.007 225	This work
$5^1\Sigma^+$	20.50	1555	30 911	16.80	0.05	0.004 652	This work
$2^3\Sigma^+$	9.20	6470	11 991	58.92	0.13	0.023 098	This work
$2^3\Sigma^+$	8.59	−112	21 033	53.91	6.48	0.026 495	This work
2nd min	18.46	324	20 594	12.77	0.13	0.005 737	This work
$3^3\Sigma^+$	12.65	849	23 093	54.35	0.87	0.012 2217	This work
$4^3\Sigma^+$	18.88	2177	30 287	19.54	0.04	0.005 485	This work
$1^1\Pi$	8.60	3049	22 418	46.96	0.18	0.026 433	This work
$2^1\Pi$	8.58	1678	24 842	49.23	0.36	0.026 557	This work
$3^1\Pi$	16.24	505	31 970	13.42	0.09	0.007 413	This work
$1^3\Pi$	7.49	2941	15 528	68.65	0.40	0.034 849	This work
$3^3\Pi$	8.99	2534	21 405	51.33	0.26	0.024 190	This work
$3^3\Pi$	15.49	621	31 854	15.32	0.09	0.008 184	This work
$1^1\Delta$	8.62	3468	22 006	55.47	0.22	0.026 311	This work
$1^3\Delta$	8.69	2682	21 264	53.13	0.26	0.025 889	This work

case of the CaRb^+ molecular ion, the present results also agree well with the results of references [35, 61, 62].

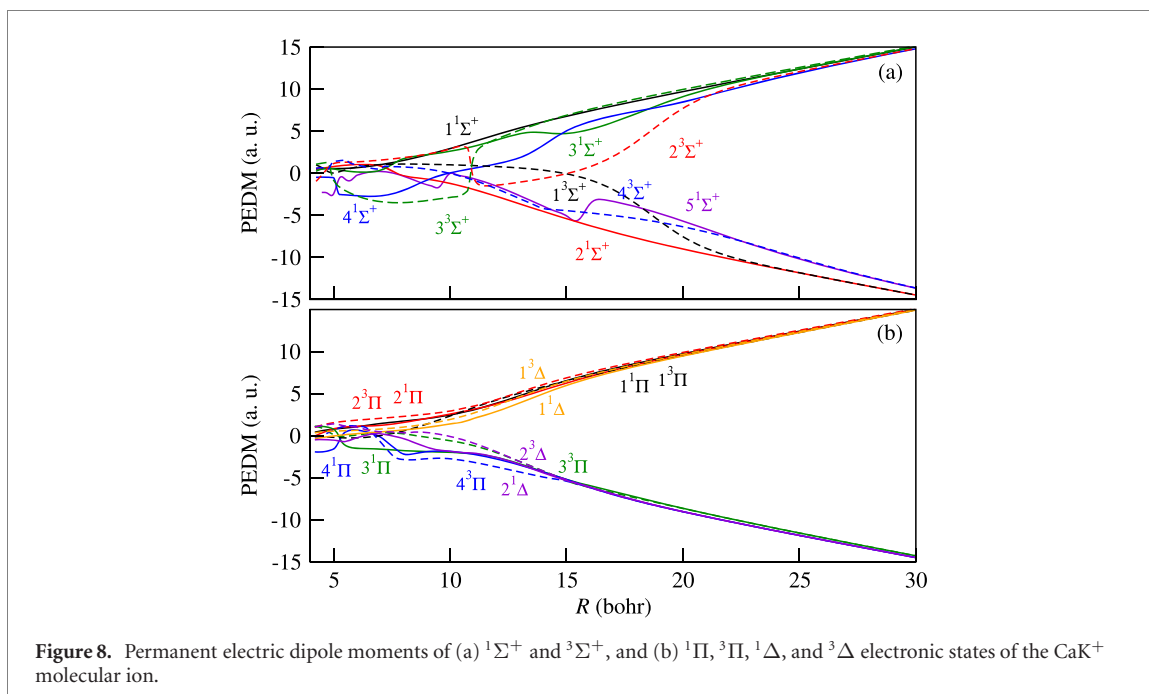
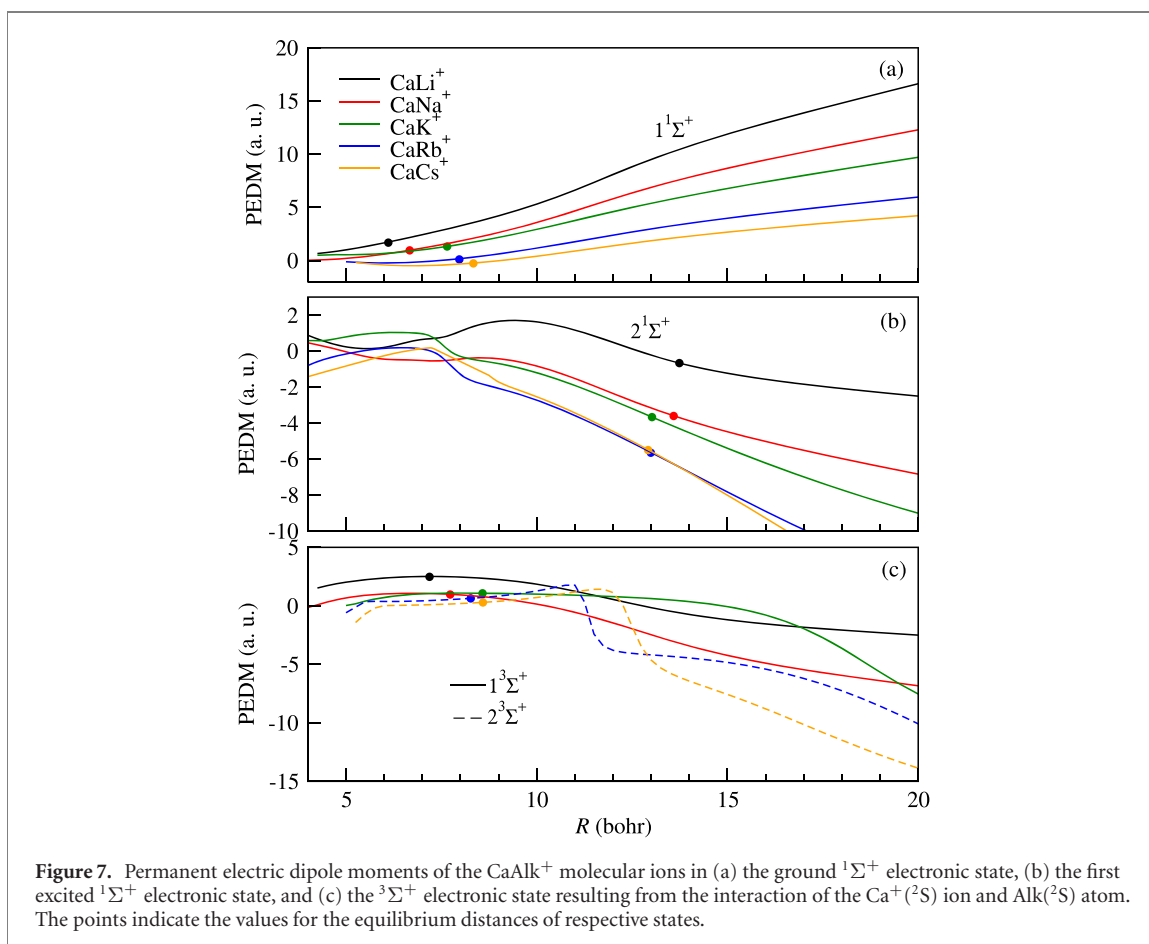
The overall good agreement between the present and previous calculations for the CaLi^+ , CaNa^+ , and CaRb^+ molecular ions suggests that similar accuracy may be expected for our results for the CaK^+ and CaCs^+ molecular ions, which have not yet been studied. Electronic structure data for the CaLi^+ , CaNa^+ , and CaRb^+ molecular ions were successfully employed to guide and interpret experimental measurements [15, 21, 24–26, 48–50]. Presented potential energy curves for the CaK^+ and CaCs^+ molecular ions may correspondingly find similar applications, e.g., in the context of experimental studies of a mixture of laser-cooled Ca^+ ions in a linear Paul trap overlapped with ultracold K atoms in a magneto-optical trap as presented recently in reference [28].

3.2. Permanent and transition electric dipole moments

The permanent and transition electric dipole moments (PEDMs and TEDMs) determine the interaction of atomic and molecular systems with static and dynamic electric fields, including the laser field. Thus, their knowledge is essential for predicting molecular spectra, lifetimes, and formation schemes. Here, we calculate permanent electric dipole moments for all investigated electronic states of the CaLi^+ , CaNa^+ , CaK^+ , CaRb^+ , and CaCs^+ molecular ions, as well as all transition electric dipole moments between electronic states of the same spin and spatial symmetries.

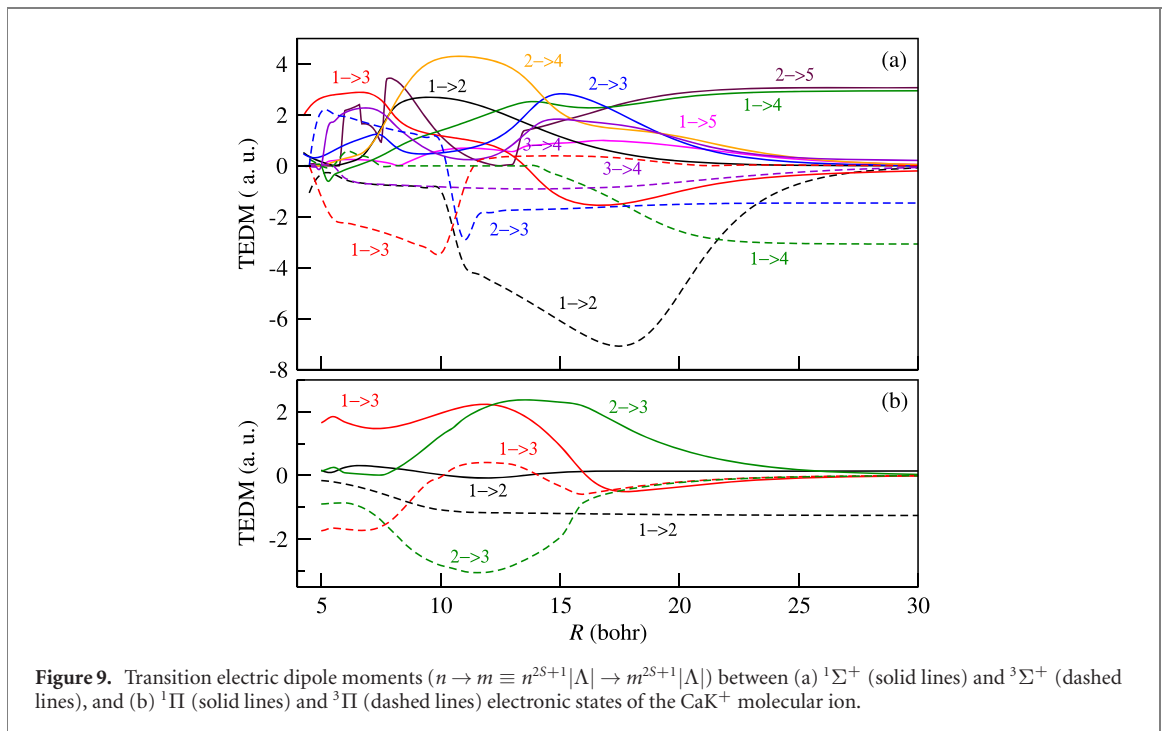
Transition electric dipole moments between the two lowest $1^1\Sigma^+$ states of the CaAlk^+ molecular ions are presented in figure 1(c). Their functions have quite similar shapes and values. They govern the radiative charge-transfer and association processes in ground-state collisions between Ca^+ ions and alkali-metal atoms which are studied in section 3.4.

Permanent electric dipole moments of the two lowest $1^1\Sigma^+$ electronic states, i.e., $1^1\Sigma^+$ states dissociating into the $\text{Ca}(1\text{S}) + \text{Alk}^+(1\text{S})$ and $\text{Ca}^+(2\text{S}) + \text{Alk}(2\text{S})$ atomic thresholds, and of the $3^3\Sigma^+$ electronic state associated with the $\text{Ca}^+(2\text{S}) + \text{Alk}(2\text{S})$ atomic threshold are presented in figure 7 for all investigated molecular ions. Values of the permanent electric dipole moments for charged molecules depend on the choice of the coordinate-system origin. Here, they are calculated with respect to the center of mass, which is a natural choice for investigating the rovibrational dynamics. Their absolute values increase with increasing internuclear distance and asymptotically approach the limiting cases where the charge is completely localized at one of the atoms. This behavior is typical for heteronuclear molecular ions and implies that even molecular ions in very weakly bound states have effectively a significant permanent electric dipole moment in contrast to neutral molecules [82, 88, 89]. The difference between the calculated values and the limiting cases is the interaction-induced variation of the permanent electric dipole moment or, in other words, the degree of charge delocalization. The limiting cases limit possible values of the dipole moment. The interatomic interaction always decreases the absolute value of the permanent electric dipole moment. The change of the sign of the dipole moment, as compared to the limiting case, means that the center of charge moved to the another side of the center of mass. Curves for the $1^1\Sigma^+$ electronic states are smooth and their asymptotic behaviors reflect the change of the center-of-mass position for different molecular ions. The degree of charge delocalization increases with the mass of the alkali-metal atom according to the



increasing difference of the electronegativity of the Ca and alkali-metal atoms. Different asymptotic behaviors for the $1^1\Sigma^+$ and $2^1\Sigma^+$ states reflect the different charge localization for the $\text{Ca}(^1S) + \text{Alk}^+(^1S)$ and $\text{Ca}^+(^2S) + \text{Alk}(^2S)$ atomic thresholds. Curves for the $3^3\Sigma^+$ electronic state of the CaRb^+ and CaCs^+ molecular ions show irregularities due to avoided crossings with nearby-lying states.

Permanent electric dipole moments of all investigated electronic states of the CaK^+ molecular ion are presented in figure 8, while transition electric dipole moments between electronic states of this molecular



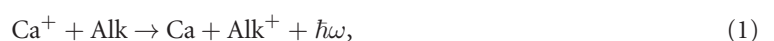
ion are plotted in figure 9. PEDMs and TEDMs for other studied molecular ions are collected in supplemental material (<https://stacks.iop.org/NJP/22/073015/mmedia>). For PEDMs, two families of curves associated with two possible arrangements of the charge at the $\text{Ca}^+ + \text{Alk}$ and $\text{Ca} + \text{Alk}^+$ atomic thresholds can be identified. The short-range deviations from the asymptotic behavior give information about charge exchange and delocalization due to interatomic interactions. The swap of the dipole moment direction via electronic excitation may potentially be a useful concept for molecular control and spectroscopy. The shapes of calculated PEDM and TEDM curves and their irregularities at short-range distances can be directly associated with avoided crossings between corresponding potential energy curves, which confirms strong interactions between involved electronic states. The knowledge of changing physical character of electronic states may be useful to predict and explain channels of non-radiative charge-transfer processes. TEDMs at large distances drop to zero when two associated atomic thresholds have different charge arrangements or related atomic excitations are dipole-forbidden. They asymptotically tend to the atomic values only in case of atomic thresholds connected by dipole-allowed transitions.

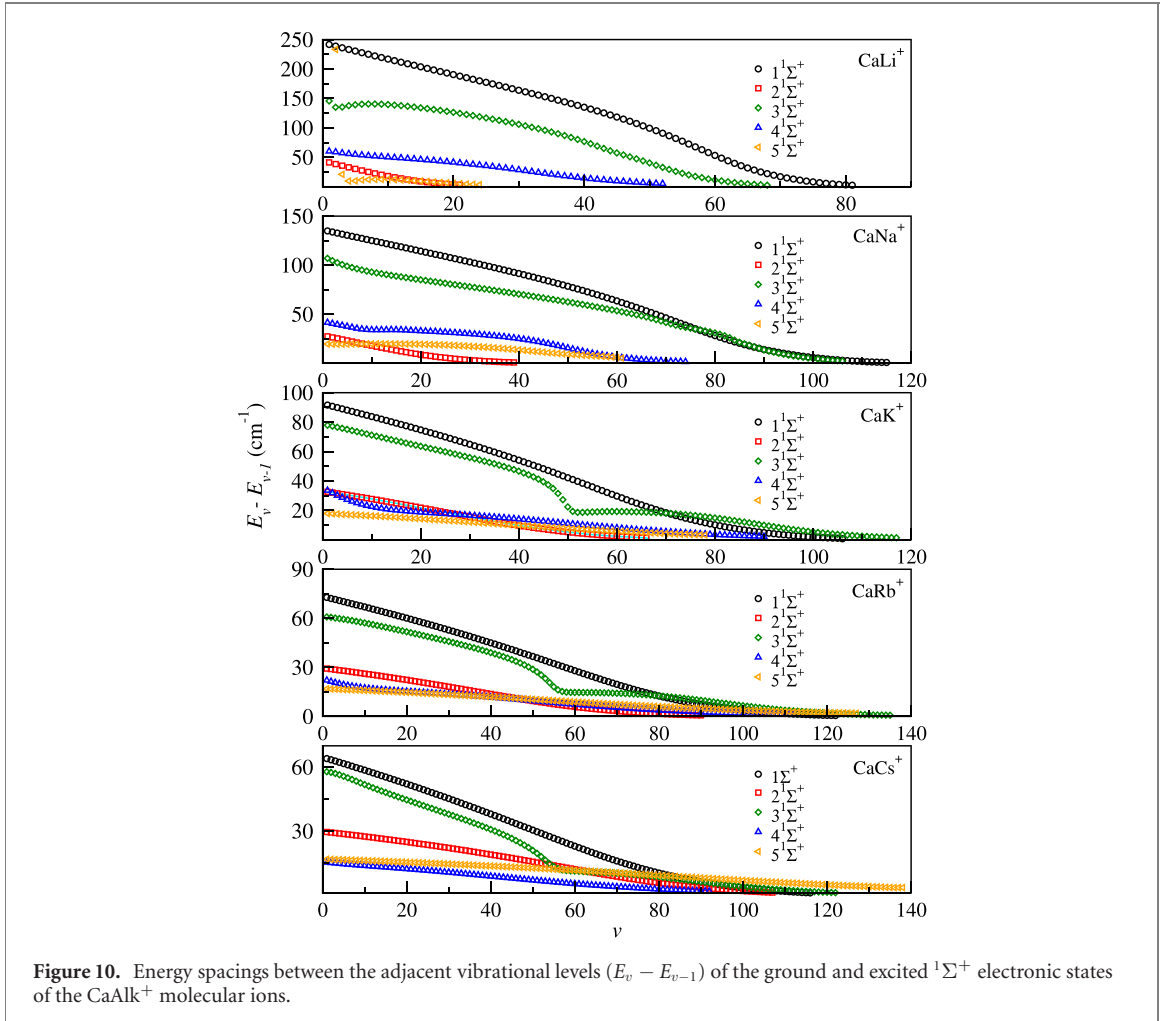
3.3. Vibrational levels

We use the present PECs to calculate corresponding vibrational states. In figure 10, we present the energy spacings between the adjacent vibrational levels ($E_v - E_{v-1}$) of the ground and excited $1\Sigma^+$ electronic states of the investigated CaAlk^+ molecular ions. For the ground electronic state, there are 86, 103, 114, 125, and 126 vibrational levels for the CaLi^+ , CaNa^+ , CaK^+ , CaRb^+ , and CaCs^+ molecular ions, respectively. The number of vibrational levels increases with the mass of the involved alkali-metal atom, despite the decreasing potential well depth (see figure 1(b)), because the effect of the increasing mass dominates. The spacing between vibrational levels diminishes gradually with a vibrational energy that reflects the strong anharmonicity of the PECs. The overall pattern of energy spacings of different electronic states for different molecular ions is similar. For some states, however, irregularities related to the avoided crossings are visible, e.g., for the $3^1\Sigma^+$ state of CaK^+ , CaRb^+ , and CaCs^+ . The inclusion of relativistic spin-orbit couplings between non-relativistic electronic states, inducing avoided crossings, may severely perturb the observed progression of vibrational states.

3.4. Spontaneous and light-assisted ion-neutral charge-transfer processes

Interactions and collisions of laser-cooled trapped Ca^+ ions with ultracold alkali-metal atoms are of the highest importance for experimental realizations of ultracold ion-atom mixtures [10, 15, 21, 24–26, 28, 48–50]. Even if both the Ca^+ ion and alkali-metal atom are in their electronic ground states, the collision- and interaction-induced radiative charge rearrangement is possible in the form of the radiative charge transfer (RCT)





where the electron is spontaneously transferred from the alkali-metal atom to the Ca^+ ion emitting a photon of energy $\hbar\omega$ and the radiative association (RA)



where the CaAlk^+ molecular ion in the (v, j) ro-vibrational level of the electronic ground state is spontaneously formed.

The interaction between the ground-state Ca^+ ion and alkali-metal atom both in the $1\Sigma^+$ and in the $3\Sigma^+$ states at large distances is dominated by the induction term

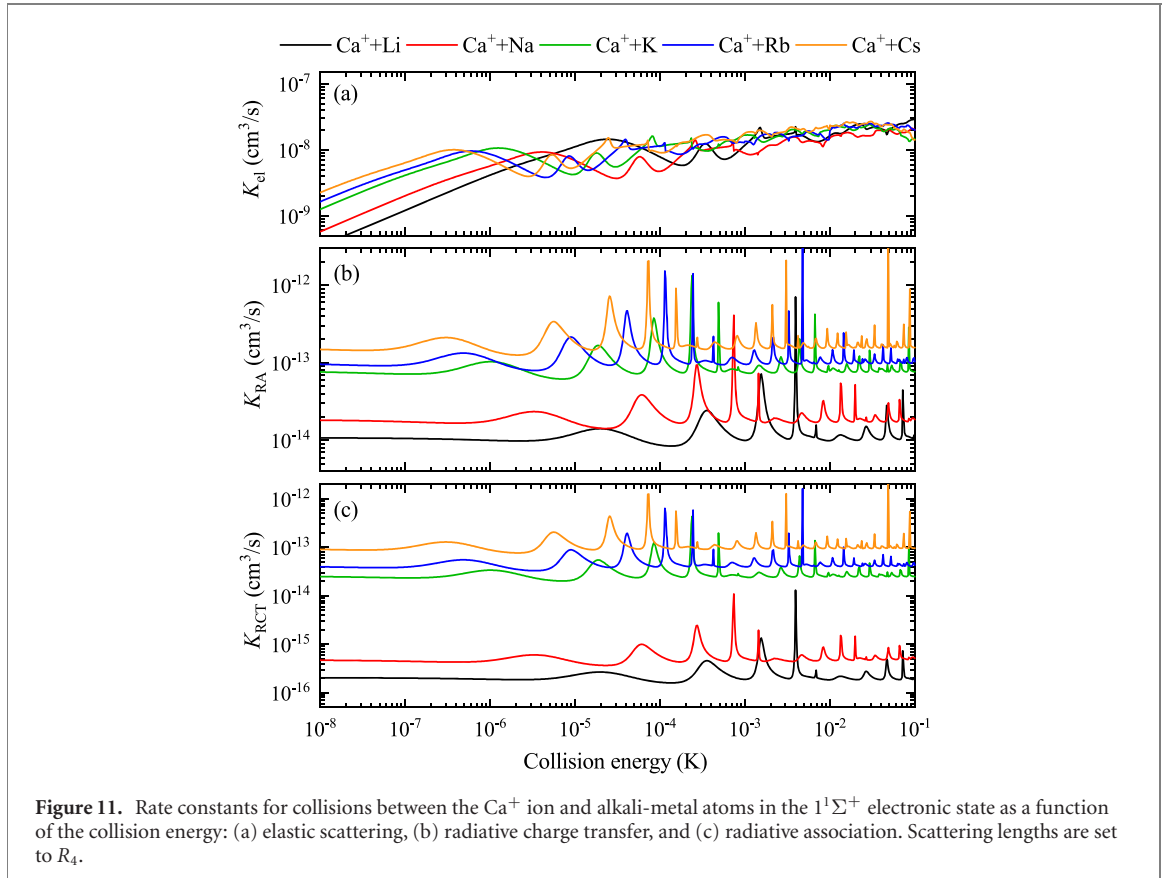
$$V(R) \underset{R \rightarrow \infty}{=} -\frac{C_4}{R^4}, \quad (3)$$

where the leading long-range induction coefficient $C_4 = \frac{1}{2}e^2\alpha_{\text{Alk}}$ is given by the static electric dipole polarizability of the alkali-metal atom α_{Alk} . This long-range interaction determines the characteristic length scale $R_4 = \sqrt{2\mu C_4/\hbar^2}$ and the related characteristic energy scale $E_4 = \hbar^2/2\mu R_4^2$ [1]. These quantities are relevant for ultracold ion–atom collisions because the length scale R_4 establishes the order of magnitude of typical ion–atom scattering lengths while the energy scale E_4 determines the quantum regime of s-wave collisions [8]. Table 7 collects the long-range coefficients, characteristic lengths, and characteristic energies of the ground-state ion–atom interaction for the investigated mixtures. The characteristic lengths are from 1337 bohr for $\text{Ca}^+ + \text{Li}$ to 4706 bohr for $\text{Ca}^+ + \text{Cs}$, and they are an order of magnitude larger for ion–atom systems as compared with neutral counterparts. The characteristic energies are from 0.13 μK for $\text{Ca}^+ + \text{Cs}$ to 8.12 μK for $\text{Ca}^+ + \text{Li}$, and they are two orders of magnitude smaller as compared with neutral counterparts. This is one of the reasons, together with inelastic losses and micromotion-induced heating in the Paul trap [51], why the realization of ion–atom collisions in the quantum regime is very challenging [8].

To produce and study the considered ion–atom mixtures in the quantum regime, the ion, after initial laser cooling, should be subsequently cooled sympathetically via elastic collisions with surrounding ultracold neutral gas [8, 29, 50]. Such a scheme is feasible only if rates for elastic scattering are significantly

Table 7. Long-range coefficients C_4 , characteristic lengths R_4 , and characteristic energies E_4 of the ground-state ion–atom induction interaction for the investigated mixtures.

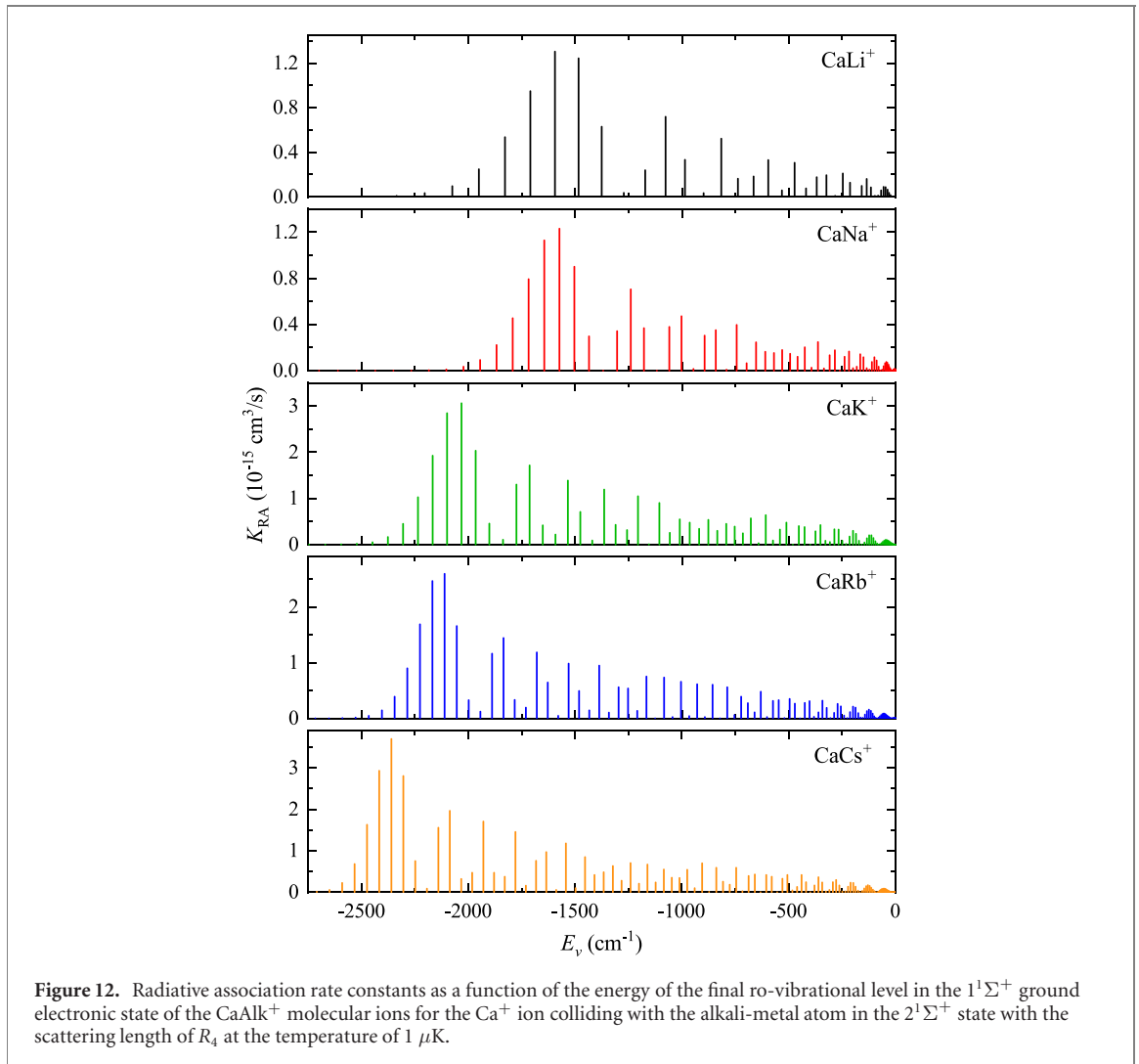
System	C_4 (a.u.)	R_4 (bohr)	E_4 (μK)
$^{40}\text{Ca}^+ + ^6\text{Li}$	82.2	1337	8.12
$^{40}\text{Ca}^+ + ^{23}\text{Na}$	83.2	2104	1.34
$^{40}\text{Ca}^+ + ^{39}\text{K}$	145.4	3234	0.42
$^{40}\text{Ca}^+ + ^{85}\text{Rb}$	159.8	3978	0.20
$^{40}\text{Ca}^+ + ^{133}\text{Cs}$	197.8	4706	0.13



larger than rates for inelastic collisions. Therefore, in figure 11, we present rate constants for elastic and radiative inelastic collisions between the Ca^+ ion and alkali-metal atoms in the $2^1\Sigma^+$ electronic state as a function of the collision energy. We assume typical scattering length of $a_s = R_4$ in the entrance channel, while the results do not depend on the scattering length in the exit channel. Rate constants for small collision energies and pattern of shape resonances depend strongly on the scattering length, but the overall magnitude of rate constants does not depend on it. In the range of investigated collision energies, the rate constants for the elastic scattering K_{el} for all systems have similar values of around $10^{-8} \text{ cm}^3 \text{ s}^{-1}$. Because the same scattering length (in unites of the characteristic length) is assumed for all $\text{Ca}^+ + \text{Alk}$ mixtures, the pattern of shape resonances is very similar for all systems, however positions of shape resonances are scaled according to the characteristic energies. Similarly to other ion–atom systems [33–35, 86, 90], shape resonances are more pronounced for inelastic rate constants, however if the thermal distribution of collision energies is assumed, the thermal averaging removes energy dependence for temperatures larger than 1 mK in agreement with predictions of the classical Langevin capture theory [91]. The magnitude of the rate constants for the radiative association K_{RA} and charge transfer K_{RCT} depends on the system. In table 8, we collect thermally averaged rate constants for the radiative association and radiative charge-transfer collisions in the investigated mixtures compared with the Langevin rate constants $K_{\text{L}} = 2\pi\sqrt{2C_4/\mu}$. Similarly as for other alkaline-earth-metal–alkali-metal ion–atom systems [15, 34, 35], the rate constants for the radiative losses are at least 10^4 times smaller than Langevin and elastic rate constants. The radiative rates constants increase with the mass of the alkali-metal atom according to the increasing energy of an emitted photon. At

Table 8. Rate constants for the Langevin K_L , radiative association K_{RA} , and radiative charge-transfer K_{RCT} collisions in the investigated mixtures.

System	K_L ($\text{cm}^3 \text{s}^{-1}$)	K_{RA} ($\text{cm}^3 \text{s}^{-1}$)	K_{RCT} ($\text{cm}^3 \text{s}^{-1}$)
$^{40}\text{Ca}^+ + ^6\text{Li}$	4.73×10^{-9}	1.29×10^{-14}	2.42×10^{-16}
$^{40}\text{Ca}^+ + ^{23}\text{Na}$	3.04×10^{-9}	2.09×10^{-14}	5.46×10^{-16}
$^{40}\text{Ca}^+ + ^{39}\text{K}$	3.46×10^{-9}	9.06×10^{-14}	2.97×10^{-14}
$^{40}\text{Ca}^+ + ^{85}\text{Rb}$	3.09×10^{-9}	1.22×10^{-13}	5.05×10^{-14}
$^{40}\text{Ca}^+ + ^{133}\text{Cs}$	3.23×10^{-9}	1.94×10^{-13}	1.18×10^{-13}

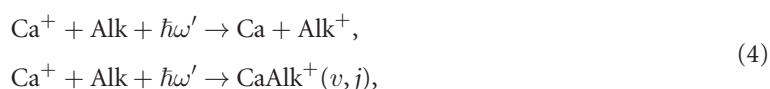
**Figure 12.** Radiative association rate constants as a function of the energy of the final ro-vibrational level in the $1^1\Sigma^+$ ground electronic state of the CaAlk^+ molecular ions for the Ca^+ ion colliding with the alkali-metal atom in the $2^1\Sigma^+$ state with the scattering length of R_4 at the temperature of $1 \mu\text{K}$.

the same time, the radiative association is 53, 38, 3.1, 2.4, and 1.6 times more probable than the radiative charge transfer for $\text{Ca}^+ + \text{Li}$, $\text{Ca}^+ + \text{Na}$, $\text{Ca}^+ + \text{K}$, $\text{Ca}^+ + \text{Rb}$, and $\text{Ca}^+ + \text{Cs}$ collisions, respectively.

Radiative association rate constants as a function of the energy of the final ro-vibrational level in the $1^1\Sigma^+$ electronic ground state for the Ca^+ ion colliding with the alkali-metal atoms in the $2^1\Sigma^+$ state are presented in figure 12. For all systems, the formation of molecular ions in vibrational levels from the middle of the spectrum is the most probable. For example, the formation of molecular ions in vibrational levels with the vibrational quantum number around $v = 46$, $v = 28$, and $v = 13$ and the binding energy around 1595 cm^{-1} , 2033 cm^{-1} , and 2361 cm^{-1} are the most probable for CaLi^+ , CaK^+ , and CaCs^+ , respectively. The molecular formation probability decreases gradually for decreasing binding energies and is strongly suppressed for binding energies larger than 2500 cm^{-1} because of the interplay between Franck–Condon factors between vibrational levels of the $1^1\Sigma^+$ and $2^1\Sigma^+$ electronic states and transition electric dipole moment between them (see figure 1). Interestingly, more deeply bound molecular ions can be formed for heavier alkali-metal atom despite their smaller potential well depths.

In a field-free case, where all spin orientations are present, the described above reactive collisions governed by the $2^1\Sigma^+$ electronic state constitute 25% of scattering. Remaining collisions are governed by the $3^3\Sigma^+$ state, which for $\text{Ca}^+ + \text{Li}$, $\text{Ca}^+ + \text{Na}$, and $\text{Ca}^+ + \text{K}$ is free from radiative losses. For $\text{Ca}^+ + \text{Rb}$ and $\text{Ca}^+ + \text{Cs}$ the radiative losses are also possible from the $3^3\Sigma^+$ state but they should be much less probable than radiative losses from the $1^1\Sigma^+$ state because of much smaller energies of realized photons. The radiative association and charge transfer are expected to be a dominant loss mechanism for the ground-state $\text{Ca}^+ + \text{Li}$ and $\text{Ca}^+ + \text{Na}$ collisions, because the entrance atomic threshold is well separated from lower and higher lying electronic states in these systems. In the case of $\text{Ca}^+ + \text{K}$ collisions, the radiative processes should also be most important however the coupling with the $1^3\Pi$ state may affect them. In the case of $\text{Ca}^+(^2\text{S}) + \text{Rb}(^2\text{S})$ collisions, nonradiative charge-transfer losses were observed [21, 61] as a dominant mechanism because of strong nonadiabatic couplings with below nearby-lying electronic states associated with the $\text{Ca}(^3\text{P}) + \text{Rb}^+(^1\text{S})$ atomic threshold. In the case of $\text{Ca}^+ + \text{Cs}$ collisions, more balanced interplay between radiative and nonradiative processes can be expected. Detailed studies of the nonradiative collisional dynamics are out of the scope of this paper.

If the Ca^+ ions or alkali-metal atoms are excited by a laser field, the light-induced charge-transfer and association processes are possible



where a laser field can be employed to directly stimulate the transition to the ground electronic state [34, 37] or to excite the ion–atom system to higher excited states [36]. In the latter case, both radiative and nonradiative deexcitation processes can happen depending on the structure of excited electronic states. Nonradiative deexcitation can be driven by nonadiabatic couplings between electronic states of the same symmetry or spin–orbit couplings between electronic states of different symmetry. If the ion–atom system is excited to higher-lying atomic thresholds, then the sequence of radiative and nonradiative deexcitations through intermediate excited electronic states can also be envisioned [36].

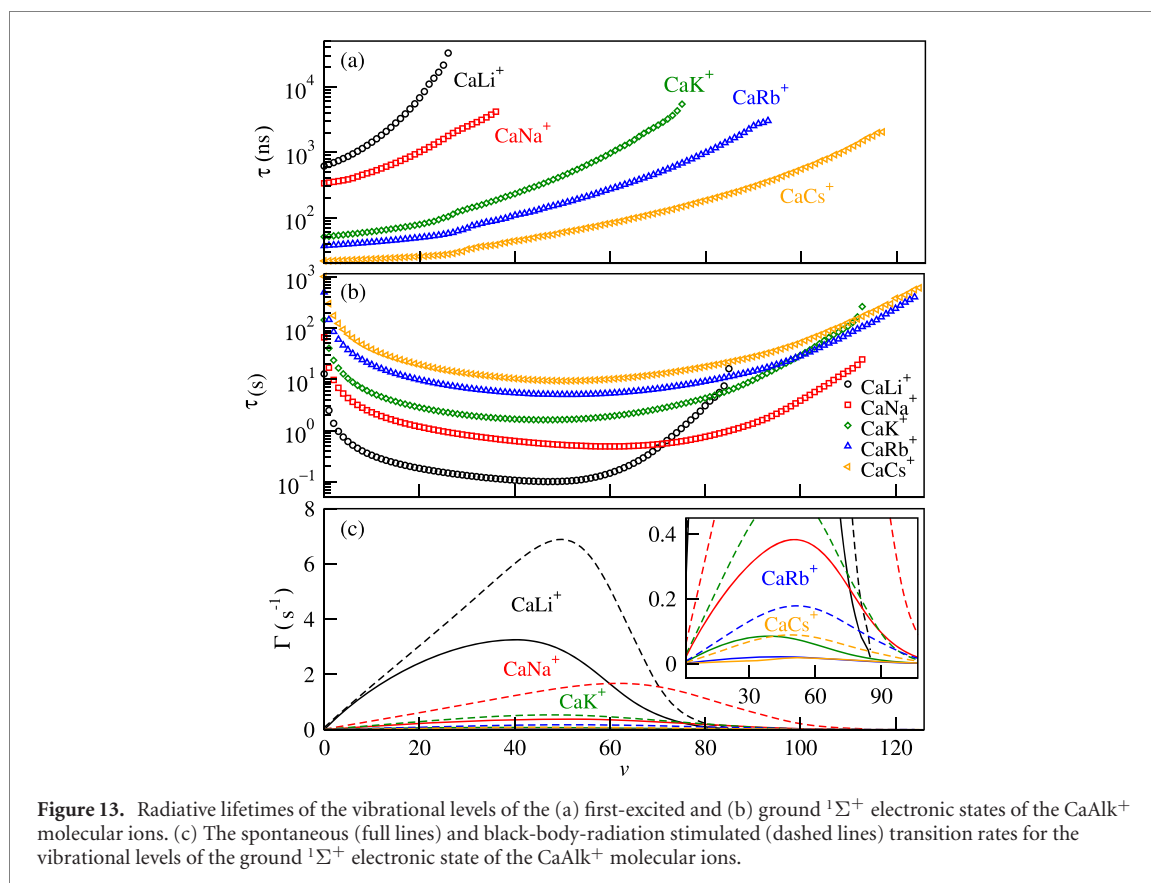
The calculated potential energy curves and transition electric dipole moments can be employed to predict and interpret experimental measurements. Various rate constants for charge-transfer collisions between excited-state Ca^+ ions and Li [15], Na [26], and Rb [21] atoms were measured and rationalized based on the structure of real and avoided crossings between involved molecular electronic states at short distances. For all investigated systems, exciting both the Ca^+ ion to the 2^2D or 2^2P states and alkali-metal atom to the 2^2P state significantly enhances the charge-transfer rate constants from negligible to significant fraction of the Langevin rate constant. For example, in figures 2 and 3, the $\text{Ca}^+(^2\text{D}) + \text{Li}(^2\text{S})$ and $\text{Ca}^+(^2\text{D}) + \text{Na}(^2\text{S})$ atomic thresholds and associated molecular electronic states are closely surrounded by several electronic states. Similar light-assisted enhancements of charge transfer can also be expected for $\text{Ca}^+ + \text{K}$ and $\text{Ca}^+ + \text{Cs}$ collisions.

The interplay between photoassociation into excited weakly bound molecular ions and subsequent deexcitation to the ground-state molecular ions or competitive dissociative charge transfer can be expected for collisions in the laser field [34, 36, 37]. The $\text{Ca}^+(^2\text{S}) + \text{Alk}(^2\text{P})$ atomic thresholds are relatively well separated from other thresholds in the considered systems. This opens the way for photoassociation spectroscopy and molecular ion formation similar as in alkali-metal gases [92]. The existence of several charge-transferred atomic thresholds may also allow for short-range photoassociation schemes. For example, the $\text{Ca}(^3\text{P}) + \text{Li}^+(^1\text{S})$ and $\text{Ca}(^3\text{P}) + \text{Na}^+(^1\text{S})$ atomic thresholds are well separated from other asymptotes, and the relevant $1^3\Sigma^+$ and $2^3\Sigma^+$ electronic states have a similar shape and are connected by the large transition dipole moment at the short range. Finally, magnetic Feshbach resonances in the ground electronic state can be employed to enhance molecular ion formation rates. Detailed studies of the photoassociation and magnetoassociation schemes, however, are out of the scope of this paper.

3.5. Radiative lifetimes

We use the present PECs, PEDMs, and TEDMs to calculate the lifetimes of vibrational states of the ground and first excited $1^1\Sigma^+$ electronic states of the considered CaAlk^+ molecular ions. These lifetimes may be useful to assess prospect for the formation and spectroscopy of calcium–alkali-metal-atom molecular ions in modern experiments with cold ion–atom mixtures.

The lifetimes of vibrational levels of the first excited $1^1\Sigma^+$ electronic state are presented in figure 13(a) and are governed by the transition electric dipole moment to the ground electronic state associated with emitting an optical photon. This transition moment is significant at short internuclear distances and decreases exponentially with the increasing internuclear distance (see figure 1(c)). Therefore, the lowest vibrational levels have lifetimes in the range of tens to hundreds of nanosecond (between 22 ns for CaCs^+



and 335 ns for CaLi^+ for the lowest vibrational level), while the most weakly bound levels have lifetimes exceeding microseconds. The lifetimes increase with the vibrational number and decrease with the increasing mass of the alkali-metal atom.

The lifetimes of vibrational levels of the ground $^1\Sigma^+$ electronic state are presented in figure 13(b) and are governed by its permanent electric dipole moment responsible for weak transitions between different vibrational levels associated with emitting microwave photons. In the case of these transitions, both relatively weak spontaneous emission and stimulated by the black body radiation absorption and emission have to be included. We assume the black body radiation spectrum with the temperature of 300 K. The lifetimes of the lowest and the most-weakly-bound vibrational levels exceed ten seconds (between 13 s for CaLi^+ and 1014 s CaCs^+ for the lowest vibrational level), while other levels have lifetimes of the order of one second. The interplay between the spontaneous and stimulated transitions can be seen in figure 13(c), where we compare the spontaneous and stimulated transition rates for the vibrational levels of the ground $^1\Sigma^+$ electronic state of the CaAlk^+ molecular ions. The present lifetimes have similar characteristics as comparable results for other neutral and ionic dimers [93, 94].

4. Conclusion

Motivated by recent experimental studies on ultracold mixtures of Ca^+ ions immersed in alkali-metal atoms, in a comparative study, we have investigated the electronic structure and the prospects for the formation of the molecular ions composed of a calcium ion and an alkali-metal atom: CaAlk^+ ($\text{Alk} = \text{Li}, \text{Na}, \text{K}, \text{Rb}, \text{Cs}$). We have used the theoretical quantum chemistry approach based on non-empirical pseudopotentials, operatorial core-valence correlation, large Gaussian basis sets, and full configuration interaction method for valence electrons. We have calculated adiabatic potential energy curves, spectroscopic constants, and transition as well as permanent electric dipole moments for the ground and several excited singlet and triplet electronic states of the Σ^+ , Π , and Δ spatial symmetries. Next, the electronic structure data have been employed to examine the prospects for the ion-neutral reactive processes and production of molecular ions via spontaneous radiative association and laser-induced photoassociation. Finally, we have calculated the radiative lifetimes of vibrational states of the ground and first excited electronic states.

Our results are in good agreement with the previous theoretical studies of the electronic structure of the ground and excited electronic states of the CaLi^+ [15, 53–58], CaNa^+ [10, 53, 59, 60], and CaRb^+ [35, 53, 61, 62] molecular ions, which confirms the accuracy of the employed computational approach. The structure of the excited electronic states of the CaK^+ and CaCs^+ molecular ions is reported here for the first time. The rate constants for the radiative charge transfer and association in the ground-state collisions of the Ca^+ ion and alkali-metal atom are predicted to be much smaller than the rate constants for elastic scattering for all the considered systems. They are also predicted to increase with the mass of the alkali-metal atom. For the ground-state $\text{Ca}^+ + \text{K}$ collisions, radiative losses should be the main source of losses, negligible for buffer gas cooling or other applications. For the ground-state $\text{Ca}^+ + \text{Cs}$ collisions, the interplay between radiative and nonradiative charger-transfer processes is expected. The radiative association leads to the formation of ground-state molecular ions with binding vibrational energies in the range of $1500\text{--}2500\text{ cm}^{-1}$ and is predicted to be more probable than radiative charge transfer. For all the systems, the excited-state inelastic collisions are expected to be much faster than the ground-state ones. Based on the electronic structure, photoassociation schemes based on both short-range and long-range excitations can be envisioned. The radiative lifetimes of vibrational states of the ground and first excited electronic states are found in the range of $0.1\text{--}100\text{ s}$ and 10 ns to $10\text{ }\mu\text{s}$, respectively. The present results may be useful and pave the way for the formation and spectroscopy of calcium–alkali-metal-atom molecular ions in modern experiments with cold ion–atom mixtures or by the ionization of their neutral counterparts. In the future, the presented computational scheme will be employed to study excited electronic states in triatomic molecular ions.

The full potential energy curves, permanent and transition electric dipole moments as a function of interatomic distance in the numerical form are available for all investigated systems from the authors upon request.

Acknowledgments

MT was supported by the National Science Centre Poland (Sonata Grant No. 2015/19/D/ST4/02173), the Foundation for Polish Science within the First Team programme cofinanced by the European Union under the European Regional Development Fund, and PL-Grid Infrastructure.

ORCID iDs

Hamid Berriche  <https://orcid.org/0000-0002-1442-669X>

Michał Tomza  <https://orcid.org/0000-0003-1792-8043>

References

- [1] Tomza M, Jachymski K, Gerritsma R, Negretti A, Calarco T, Idziaszek Z and Julienne P S 2019 *Rev. Mod. Phys.* **91** 035001
- [2] Côté R 2016 *Adv. At. Mol. Opt. Phys.* **65** 67
- [3] Härter A and Denschlag J H 2014 *Contemp. Phys.* **55** 33
- [4] Côté R and Dalgarno A 2000 *Phys. Rev. A* **62** 012709
- [5] Zipkes C, Palzer S, Sias C and Köhl M 2010 *Nature* **464** 388
- [6] Ravi K, Lee S, Sharma A, Werth G and Rangwala S 2012 *Nat. Commun.* **3** 1126
- [7] Höltkemeier B, Weckesser P, López-Carrera H and Weidemüller M 2016 *Phys. Rev. Lett.* **116** 233003
- [8] Feldker T, Fürst H, Hirzler H, Ewald N, Mazzanti M, Wiater D, Tomza M and Gerritsma R 2020 *Nat. Phys.* **16** 413
- [9] Sikorsky T, Meir Z, Ben-shlomi R, Akerman N and Ozeri R 2018 *Nat. Commun.* **9** 920
- [10] Makarov O P, Côté R, Michels H and Smith W W 2003 *Phys. Rev. A* **67** 042705
- [11] Ratschbacher L, Zipkes C, Sias C and Kohl M 2012 *Nat. Phys.* **8** 649
- [12] Fürst H, Feldker T, Ewald N V, Joger J, Tomza M and Gerritsma R 2018 *Phys. Rev. A* **98** 012713
- [13] Sikorsky T, Morita M, Meir Z, Buchachenko A A, Ben-shlomi R, Akerman N, Narevicius E, Tscherbil T V and Ozeri R 2018 *Phys. Rev. Lett.* **121** 173402
- [14] Côté R and Simbotin I 2018 *Phys. Rev. Lett.* **121** 173401
- [15] Saito R, Haze S, Sasakawa M, Nakai R, Raoult M, Da Silva H, Dulieu O and Mukaiyama T 2017 *Phys. Rev. A* **95** 032709
- [16] Gerritsma R, Negretti A, Doerk H, Idziaszek Z, Calarco T and Schmidt-Kaler F 2012 *Phys. Rev. Lett.* **109** 080402
- [17] Bissbort U, Cocks D, Negretti A, Idziaszek Z, Calarco T, Schmidt-Kaler F, Hofstetter W and Gerritsma R 2013 *Phys. Rev. Lett.* **111** 080501
- [18] Schurer J M, Negretti A and Schmelcher P 2017 *Phys. Rev. Lett.* **119** 063001
- [19] Doerk H, Idziaszek Z and Calarco T 2010 *Phys. Rev. A* **81** 012708
- [20] Grier A T, Cetina M, Oručević F and Vuletić V 2009 *Phys. Rev. Lett.* **102** 223201
- [21] Hall F H, Eberle P, Hegi G, Raoult M, Aymar M, Dulieu O and Willitsch S 2013 *Mol. Phys.* **111** 2020
- [22] Sullivan S T, Rellergert W G, Kotochigova S and Hudson E R 2012 *Phys. Rev. Lett.* **109** 223002
- [23] Rellergert W G, Sullivan S T, Kotochigova S, Petrov A, Chen K, Schowalter S J and Hudson E R 2011 *Phys. Rev. Lett.* **107** 243201
- [24] Haze S, Hata S, Fujinaga M and Mukaiyama T 2013 *Phys. Rev. A* **87** 052715

- [25] Hall F H J, Aymar M, Bouloufa-Maafa N, Dulieu O and Willitsch S 2011 *Phys. Rev. Lett.* **107** 243202
- [26] Smith W, Goodman D, Sivarajah I, Wells J, Banerjee S, Côté R, Michels H, Montgomery J A and Narducci F 2014 *Appl. Phys. B* **114** 75
- [27] Meir Z, Sikorsky T, Ben-shlomi R, Akerman N, Dallal Y and Ozeri R 2016 *Phys. Rev. Lett.* **117** 243401
- [28] Jyothi S, Egodapitiya K N, Bondurant B, Jia Z, Pretzsch E, Chiappina P, Shu G and Brown K R 2019 *Rev. Sci. Instrum.* **90** 103201
- [29] Schmidt J, Weckesser P, Thielemann F, Schaetz T and Karpa L 2020 *Phys. Rev. Lett.* **124** 053402
- [30] Härter A, Krüchow A, Brunner A, Schnitzler W, Schmid S and Hecker Denschlag J 2012 *Phys. Rev. Lett.* **109** 123201
- [31] Singer K, Poschinger U, Murphy M, Ivanov P, Ziesel F, Calarco T and Schmidt-Kaler F 2010 *Rev. Mod. Phys.* **82** 2609
- [32] Schneider C, Porras D and Schaetz T 2012 *Rep. Prog. Phys.* **75** 024401
- [33] Idziaszek Z, Simoni A, Calarco T and Julienne P S 2011 *New J. Phys.* **13** 083005
- [34] Tomza M, Koch C P and Moszynski R 2015 *Phys. Rev. A* **91** 042706
- [35] da Silva H Jr, Raoult M, Aymar M and Dulieu O 2015 *New J. Phys.* **17** 045015
- [36] Gacesa M, Montgomery J A, Michels H H and Côté R 2016 *Phys. Rev. A* **94** 013407
- [37] Petrov A, Makrides C and Kotochigova S 2017 *J. Chem. Phys.* **146** 084304
- [38] Hall F H, Aymar M, Raoult M, Dulieu O and Willitsch S 2013 *Mol. Phys.* **111** 1683
- [39] Jyothi S, Ray T, Dutta S, Allouche A R, Vexiau R, Dulieu O and Rangwala S A 2016 *Phys. Rev. Lett.* **117** 213002
- [40] Sullivan S T, Rellergert W G, Kotochigova S, Chen K, Schowalter S J and Hudson E R 2011 *Phys. Chem. Chem. Phys.* **13** 18859
- [41] Deiglmayr J, Göritz A, Best T, Weidemüller M and Wester R 2012 *Phys. Rev. A* **86** 043438
- [42] Puri P, Mills M, Schneider C, Simbotin I, Montgomery J A, Côté R, Suits A G and Hudson E R 2017 *Science* **357** 1370
- [43] Kilaj A, Gao H, Rösch D, Rivero U, Küpper J and Willitsch S 2018 *Nat. Commun.* **9** 2096
- [44] Dörfler A D, Eberle P, Koner D, Tomza M, Meuwly M and Willitsch S 2019 *Nat. Commun.* **10** 5429
- [45] Puri P, Mills M, Simbotin I, Montgomery J A, Côté R, Schneider C, Suits A G and Hudson E R 2019 *Nat. Chem.* **11** 615
- [46] Germann M, Tong X and Willitsch S 2014 *Nat. Phys.* **10** 820
- [47] Cairncross W B, Gresh D N, Grau M, Cossel K C, Roussy T S, Ni Y, Zhou Y, Ye J and Cornell E A 2017 *Phys. Rev. Lett.* **119** 153001
- [48] Eberle P, Dörfler A D, Von Planta C, Ravi K and Willitsch S 2016 *ChemPhysChem* **17** 3769
- [49] Haze S, Saito R, Fujinaga M and Mukaiyama T 2015 *Phys. Rev. A* **91** 032709
- [50] Haze S, Sasakawa M, Saito R, Nakai R and Mukaiyama T 2018 *Phys. Rev. Lett.* **120** 043401
- [51] Cetina M, Grier A T and Vuletic V 2012 *Phys. Rev. Lett.* **109** 253201
- [52] Li H, Jyothi S, Li M, Klos J, Petrov A, Brown K R and Kotochigova S 2020 *Phys. Chem. Chem. Phys.* **22** 10870
- [53] Śmiałkowski M and Tomza M 2020 *Phys. Rev. A* **101** 012501
- [54] Bala R, Nataraj H, Abe M and Kajita M 2019 *Mol. Phys.* **117** 712
- [55] Habli H, Mejrissi L, Ghalla H, Yaghmour S J, Oujia B and Gadéa F X 2016 *Mol. Phys.* **114** 1568
- [56] Xie R-H and Gong J 2005 *Phys. Rev. Lett.* **95** 263202
- [57] Russon L, Rothschof G, Morse M, Boldyrev A and Simons J 1998 *J. Chem. Phys.* **109** 6655
- [58] Kimura M, Sato H and Olson R 1983 *Phys. Rev. A* **28** 2085
- [59] Gacesa M, Montgomery J A Jr, Michels H H and Côté R 2016 *Phys. Rev. A* **94** 013407
- [60] Jellali S, Habli H, Mejrissi L, Hamdi R, Oujia B and Gadéa F X 2018 *J. Quant. Spectrosc. Radiat. Transfer* **209** 45
- [61] Tacconi M, Gianturco F and Belyaev A 2011 *Phys. Chem. Chem. Phys.* **13** 19156–64
- [62] Hall F H, Eberle P, Hegi G, Raoult M, Aymar M, Dulieu O and Willitsch S 2013 *Mol. Phys.* **111** 2020
- [63] Pototschnig J V, Meyer R, Hauser A W and Ernst W E 2017 *Phys. Rev. A* **95** 022501
- [64] Berriche H 1995 Etude spectroscopique *ab initio* de LiH et LiH⁺ au-delà de l'approximation de Born Oppenheimer *PhD Thesis* Paul Sabatier University (unpublished)
- [65] Khelifi N, Zrafi W, Oujia B and Gadea F X 2002 *Phys. Rev. A* **65** 425131
- [66] Zrafi W, Oujia B and Gadea F X 2006 *J. Phys. B: At. Mol. Opt. Phys.* **39** 3815
- [67] Khelifi N, Oujia B and Gadea F X 2001 *J. Chem. Phys.* **116** 2879
- [68] Mabrouk N and Berriche H 2014 *J. Phys. Chem A* **118** 8828–41
- [69] Mabrouk N and Berriche H 2008 *J. Phys. B: At. Mol. Opt. Phys.* **41** 155101
- [70] Mabrouk N, Berriche H, Ouada H B and Gadea F 2010 *J. Phys. Chem. A* **114** 6657
- [71] Jendoubi I, Berriche H, Ben Ouada H and Gadea F 2012 *J. Phys. Chem. A* **116** 2945–60
- [72] Aymar M and Dulieu O 2012 *J. Phys. B: At. Mol. Opt. Phys.* **45** 215103
- [73] Habli H 2013 Etude spectroscopique théorique *ab-initio* au-delà de l'approximation de Born Oppenheimer de l'hydrure de calcium CaH et de son ion CaH⁺ *PhD Thesis* University of MonastirTunisia (unpublished)
- [74] Belayouni S, Ghanmi C and Berriche H 2016 *Can. J. Phys.* **94** 791
- [75] ElOualhazi R and Berriche H 2016 *J. Phys. Chem. A* **120** 452–65
- [76] Aymar M, Guérout R and Dulieu O 2011 *J. Chem. Phys.* **135** 064305
- [77] Durand P and Barthelat J-C 1975 *Chim. Acta* **38** 283–302
- [78] Müller W, Flesch J and Meyer W 1984 *J. Chem. Phys.* **80** 3297
- [79] Mitroy J and Zhang J 2008 *Eur. Phys. J. D* **46** 415
- [80] NIST atomic spectra database <http://physics.nist.gov/PhysRefData/ASD>
- [81] Johnson B R 1978 *J. Chem. Phys.* **69** 4678
- [82] Tomza M 2015 *Phys. Rev. A* **92** 062701
- [83] Zemke W T, Crooks J B and Stwalley W C 1978 *J. Chem. Phys.* **68** 4628
- [84] Partridge H and Langhoff S R 1981 *J. Chem. Phys.* **74** 2361
- [85] Pazyuk E, Stolyarov A and Pupyshev V 1994 *Chem. Phys. Lett.* **228** 219
- [86] Sayfutyarova E R, Buchachenko A A, Yakovleva S A and Belyaev A K 2013 *Phys. Rev. A* **87** 052717
- [87] Li M, Mills M, Puri P, Petrov A, Hudson E R and Kotochigova S 2019 *Phys. Rev. A* **99** 062706
- [88] Gopakumar G, Abe M, Hada M and Kajita M 2014 *J. Chem. Phys.* **140** 224303
- [89] Pototschnig J V, Hauser A W and Ernst W E 2016 *Phys. Chem. Chem. Phys.* **18** 5964
- [90] Krych M, Skomorowski W, Pawłowski F, Moszynski R and Idziaszek Z 2011 *Phys. Rev. A* **83** 032723
- [91] Levine R D 2009 *Molecular Reaction Dynamics* (Cambridge: Cambridge University Press)
- [92] Jones K M, Tiesinga E, Lett P D and Julienne P S 2006 *Rev. Mod. Phys.* **78** 483
- [93] Zemke W T and Stwalley W C 2004 *J. Chem. Phys.* **120** 88
- [94] Fedorov D A, Barnes D K and Varganov S A 2017 *J. Chem. Phys.* **147** 124304